INTERFACIAL STUDIES
USING
DROP IMAGE PROCESSING TECHNIQUES

A Thesis submitted for the Degree of
Doctor of Philosophy
at the University of Southampton
by

Hubert Hugues Jacques Girault

October 1982

Department of Chemistry

UNIVERSITY OF SOUTHAMPTON

ABSTRACT

FALCULTY OF SCIENCE

CHEMISTRY

Doctor of Philosophy

INTERFACIAL STUDIES USING DROP IMAGE PROCESSING TECHNIQUES

by Hubert Hugues Jacques Girault

A novel method for measuring the boundary tension, based on the line by line digitisation of the video image of a pendant drop, has been developed. The method is equivalent to measuring about 1000 pairs of (X,Y) coordinates of the drop profile. From this, the boundary tension can be calculated using the following computational sequence: 1) the location of the inflexion plane, 2) the calculation of the cross-sectional diameter and the slope of the tangent of the drop at the inflexion plane, 3) the calculation of the volume of fluid hanging between the inflexion plane and the apex and 4) the calculation of the boundary tension.

The first part of this thesis describes this method and its mathematical basis as well as an attempt of error analysis. A description of the image recording system, the line by line digitiser and the computing equipment used is also given, together with the complete system calibration procedure.

The second part is dedicated to the study of the ion free or compact layer at the interface between organic solvents having a low mutual miscibility with water and electrolyte solutions. Measurements of the surface excess concentration of water at the interface are carried out for alkali metal chloride solutions in contact with nitrobenzene, 1,2-dichloroethane and n-heptane. The results obtained indicate that the interface should be considered as a continuous transition region rather than a compact layer.

The final part illustrates the possibilities of using the line by line digitiser to investigate the kinetics of adsorption at the fluid-liquid interfaces. Cytochrome-c is used in this study.

To Jördis and my parents.

" Il chercha son bonheur dans l'étude de la Nature. Les vérités qu'il découvre sont à lui; il nourrit et il élève son âme; il vit tranquille; il ne craint rien des hommes ..."

Zadig. Voltaire. 1747.

Acknowledgements

This thesis is the outcome of two years spent at Southampton University and I sincerely wish to thank all those who took interest in this work. First and foremost, I would like to express my gratitude to David Schiffrin, whose communicative passion for science made this study always appear to be a race against time and, to Brian Smith who opened for us the doors to image digitisation and drop image processing technique.

I would also like to thank Leonard Berlouis and Clive Godden for their participation in this work, their friendship, and most important of all, for the good times we had. Many thanks to Tom Young, Peter Francis and Garry for their skilful advice and help in building the whole system.

I also wish to thank Mme Barbier, the Institut National polytechnique de Grenoble and the DGRST for their encouragement and help in making my visit to Southampton possible.

My special and grateful thanks goes to Mary and Graham Hills, and Marjory Schiffrin for their hospitality, their support and their friendship.

I am grateful to the SERC for their support during this study and also to all those who have contributed to develop such a good scientific environment at Southampton Universtity.

Finally, I wish to express all my loving and sincere gratitude to Jördis for ... everything, including the typing of this thesis.

INDEX

CHAPTER 1

INTRODUCTION TO THE STUDIES OF THE INTERFACE BETWEEN TWO IMMISCIBLE ELECTROLYTE SOLUTIONS

1.1. Preface

The electrified interface is an important aspect of all heterogeneous chemical systems. It is a vital feature of many biochemical systems and also of other, less complex systems including, for example, colloids, gels, artificial membranes and metal-electrolyte interfaces. The last named has been the subject of intense study and much of the language and hence our understanding of the electrified interface stems from experimental studies of the mercury-aqueous electrolyte interface.

The success of these studies derives from several factors but especially from the smoothness, the unreactivity and therefore the reproducibility of this interface. Attempts to carry over these certainties into other systems such as colloids, gels and membranes immediately meet with problems of the unknown physical structure of their surfaces and even of their unknown chemical composition.

Such drawbacks do not, however, attach to another type of interface, namely that between two immiscible liquids neither of which is a metal. Such a system is accesible to all the electrochemical techniques established to characterise the metal-solution interface and the application of some of them has been described in an earlier work[25].

These systems, i.e. those containing an " Interface between Two Immiscible Electrolyte Solutions (ITIES) " have been studied in a variety of contexts, perhaps the most important being that of solvent extraction. This chapter presents the development of the electrochemical studies and the interfacial studies of the ITIES done until today.

1.2. Electrochemical studies of ITIES

The first electrochemical experiment on the liquid-liquid interface was done as early as 1902 by Nernst and Riesenfeld[51] . They studied the electrolysis of a system composed of an inorganic electrolyte (KI_3) at partition equilibrium between the oil phase (Phenol) and the aqueous phase. They found that the passage of current through the interface caused an interfacial accumulation (or depletion) according to

$$i\,(t_+^{w} - t_+^{o})\,F = -\left(D_w \left(\frac{\partial C(w)}{\partial x}\right)_{x=0} + D_o \left(\frac{\partial C(o)}{\partial x}\right)_{x=0} \right)$$

in which i is the current density, t_+ the transport number of the cation and D the diffusion coefficient. This transport equation, which predates the better - known Sand equation for solid electrodes, does not apply in the presence of a supporting electrolyte.

After this pioneering work, the investigation of ITIES was limited, during the first half of the century, to the study of the equilibrium or rest electrical potential between an aqueous and an organic phase in the presence of various electrolytes. It was only in 1956 that Guastalla[28] studied the transfer of ions through ITIES under flow of an electrical current, i.e. under non-equilibrium conditions. He observed that in a system composed of cetyltrimethyl-ammonium bromide in water and nitrobenzene, the interfacial tension changed during the passage of the current. He called this effect "electroadsorption"[30,31] and he assumed it to be caused by the electrical field arising at the ITIES during the current flow. Similar systems were also studied by Dupeyrat[10-12] and Watanabe[70] . Later Blank[8] interpreted this electroadsorption phenomenon exclusively in terms of the accumulation or depletion of surface active electrolytes at the interface. This interpretation has been recently confirmed by Buck[49] who made an extensive numerical study of ion transfer.

In 1962, Gavach[16] and Guastalla published, for the first time, steady state polarisation curves obtained with a system of aqueous KCℓ in contact with solutions of alkyltrimethylammonium picrates in nitrobenzene. Afterwards, Gavach and his colleagues[17–22] investigated, in much detail, the ITIES using chronopotentiometric methods. They first studied the transfer of tetrabutylammonium cations from water to nitrobenzene in a system composed of an aqueous solution of tetrabutylammonium bromide, with sodium bromide in excess and tetrabutylammonium tetraphenylborate in nitrobenzene. The chronopotentiograms obtained were similar to those obtained for metal-electrolyte systems under mass transfer control. The results indicated that the tetrabutylammonium ion transfer from water to nitrobenzene was mainly controlled by diffusion and obeyed the Sand equation in the current density range studied.

Secondly, they studied a system in which no common ion existed in the two phases. In the case of aqueous potassium halide solutions in contact with hexadecyl (C_{16}) trimethylammonium picrate in nitrobenzene, the chronopotentiograms were found to be different to those observed previously. A typical representation is given in figure 1.1. Taking into account only the diffusion overvoltage ($i < 0.1\ \mu A \cdot cm^{-2}$) they determined the interfacial transport number of the picrate ion and cross-checked the results by analysis of the composition of the two phases after the electrolysis.

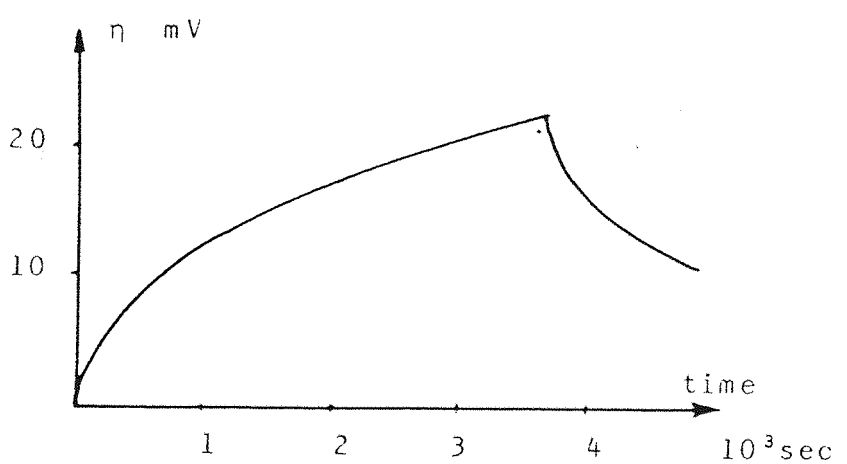

Figure 1.1

Since then, other chronopotentiometric studies of ITIES have been carried out[25,43] with different salts and different solvents and an extensive mathematical treatment of the technique has been given by R. Buck[49] .

In 1977, Gavach et al.[23,27] proposed a model for the structure of the interface between two immiscible electrolyte solutions. This model postulated the existence of a compact layer, similar to the inner layer at a metal-electrolyte interface, which would separate two classical diffuse double layers. A simple representation of this model is given in figure 1.2.

It is important to note that the use of the Gouy — Chapman treatment, i.e. ions considered as point charges and thus neglecting ion polarisation, the variation of the dielectric constant of the medium, and the effects of image forces on the standard chemical potential of the ions, results in further complication in the case of the liquid-liquid interface. Indeed, in the second integration of the Poisson equation for a diffuse double layer, it becomes difficult to integrate

$$\frac{\partial \phi(x)}{\partial x} = - \left(\frac{8kTN^{\infty}}{\varepsilon} \right)^{1/2} \sinh \frac{ze^-}{2kT} \left[\phi(x) - \phi(\infty) \right]$$

since the boundary conditions at the interface will decide the shape of the variation of the potential across the interface, in other words, a tautology is implicit in the boundary conditions established.

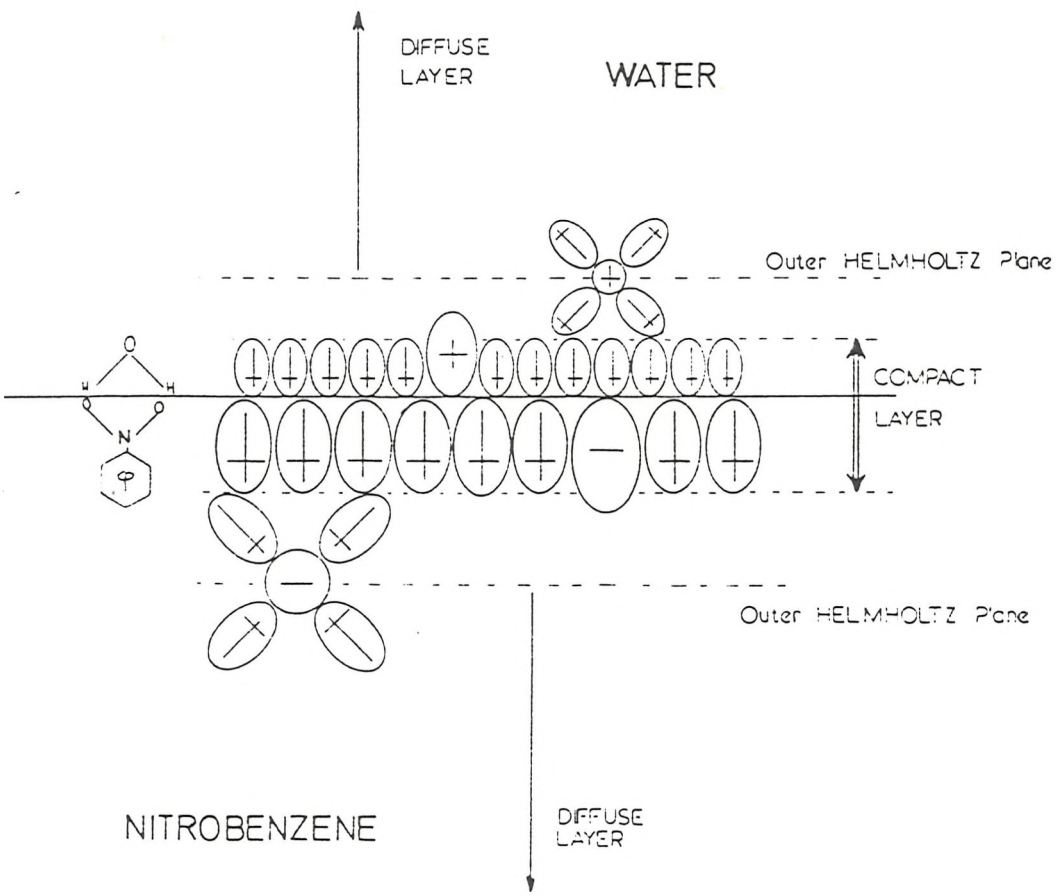

Figure 1.2: Schematic representation of the compact layer model

After this decade of investigations by Gavach, interest in this field was then shown by electrochemists. In 1976, Koryta[44-46] developed a rising electrolyte electrode similar to Heyrovsky's dropping mercury electrode. The polarograms obtained also had an S-shape and the limiting current due to the transfer of tetramethylammonium ions was found to be proportional to the concentration of the ion.

It was only with the development of a four electrode potentiostat with iR compensation, by Marecek[61] , that it was possible to monitor the potential difference across the ITIES. With this new instrument, Samec et al.[36,59-61] applied cyclic voltammetry to liquid-liquid interfaces. This technique is a very useful tool to study ion-transfer if used with systems offering a large "window" of potential[37] . These authors showed that the transfer of ions is dependent on the potential difference across the interface. A relationship between this potential difference and the ionic energy of transfer has been calculated.

The four electrode potentiostat can also be used for chronoamperometric studies, as already described in an earlier work[25] . Recently, a detailed review of the development of the electrochemical knowledge of ITIES has been published by Koryta and Vanysek[47].

1.3. Interfacial studies of ITIES

A very large part of the study of liquid-liquid interfaces centres around

a) the measurement of the interfacial tension ;
b) adhesion and adsorption.

1.3.1. Interfacial tension measurements

Nearly all the static techniques used for measuring interfacial tension have been designed during the first half of this century. These can be classified in two groups.

The first group includes the so called "detachment methods" and labels any method based on the determination of the force required to detach an object from the interface between two liquids. Amongst these methods, one can cite the Du Noüy ring[53] (1919), the Wilhelmy slide[71] (1863) and the Guastalla stirrup[29]. But these methods involve the enlarging and the breaking up of the liquid surface and therefore, are not strictly static in nature. Furthermore, their theoretical foundations are not direct functions of the interfacial tension which necessitates the introduction of correction factors that make these methods semiempirical and not accurate.

The second group comprises the methods that are connected with the properties of curved liquid interfaces. Most of them have been designed to measure surface tension rather than interfacial tension.

The capillary rise method is generally considered to be the most accurate method available for the measurement of surface tension, provided that the contact angle is kept at zero. In the case of the liquid-liquid interface however, the contact angle is seldom equal to zero, which makes its reproducibility very difficult. This drawback makes the method inadequate for interfacial tension measurements.

The drop weight is a very old method designed by Tate[65] in 1864. Unfortunately, the theory of drop detachment is still not complete, but an empirical calibration for the liquid-vapour interface has been given by Harkins and Brown[33](1919). This calibration is commonly used for the measurement of interfacial tension. The method, although not an absolute one, gives reproducible results in the case of pure components, liquid mixtures and dilute solutions of surface active agents.

The maximum bubble pressure method is mainly used to measure surface tensions. Nevertheless, it has also been used to measure the interfacial tension of mercury first by Schiffrin[63] and later in a completely computerized

version by Mohilner[50] .

These four methods are indeed not absolute methods and are dependent, to different extents, on the control of contact angles. The only absolute methods, which do not depend on the presence of a third phase, e.g. glass, are the ones based on the measurements of the geometrical dimensions of a sessile or pendant drop profile.

The pendant drop technique was developed in 1938 by Andreas and Hauser[5] . The measurement is performed by photographing a pendant drop and then determining the profile coorinates at two selected cross sectional planes. The first plane considered is usually the equatorial plane (maximum diameter) and the location of the second plane is taken as the vertical distance from the drop apex, equal in magnitude to the equatorial drop diameter. The relationship between the cross sectional diameters of these two planes has been derived empirically by Andreas et al.[5] and also by numerical integration of the corresponding differential equation by Fordham[14] and Stauffer[64] (see Chapter II). The main experimental difficulty of the method lies therefore in the accurate determination of the set of drop shape coordinates from photographic films or plates. Recently, Vos and Los[67] applied a striascopic image technique to improve the method and developed a new numerical approach which made use of about 100 drop shape coordinates. In their work, the coordinates were measured with the aid of a travelling microscope.This manual approach, although very accurate, is however as cumbersome and time consuming as the classical pendant drop analysis.

The pendant drop method has been widely used for measurements of interfacial tension. In 1952, Donahue and Bartell[9] studied water-organic liquid interfaces. Later, in 1969, Roe[58] studied interfacial tension between polymer liquids. The technique has also been used for solutions where the solute is either positively or negatively adsorbed at the interface[68] . A recent review about this technique has been published by Ambwani and Fort[3] .

1.3.2. Adhesion and adsorption

The interest in the study of adhesion of two liquids is considerable in its own right and may also throw light on problems associated with the wetting of solids by liquids. Nevertheless, the theoretical understanding of this phenomenon is not yet fully well defined. Attempts have been made to interpret adhesion in terms of molecular forces[13] but the various treatments are still semi-empirical. Even now, the state of the theory of molecular interactions at interfaces is still largely undeveloped.

On the other hand, the study of adsorption is a very old and well investigated subject. The relationship between the quantity adsorbed per unit area and the change in surface tension of a solvent produced by a solute was given in 1878 by Willard Gibbs in his comprehensive thermodynamical paper " On the Equilibrium of Heterogeneous Substances "[24]. In 1917, Langmuir[48] showed that the adsorbed films of organic substances at the surface of aqueous solutions are probably one molecule thick, with the molecules moving around independently in the films.

Since these early investigations of the adsorption phenomena, a lot of work has been carried out at the interface between two liquids. Unfortunately, most of this work has been done at the mercury-fluid interface whilst the oil-water interface has been more or less forsaken.

1.4. Presentation of the present work

The development, in an earlier work[25], of a Hanging Electrolyte Drop Electrode (similar to the Hanging Mercury Drop Electrode) allowed a better application of electrochemical techniques to the study of the Interface between Two Immiscible Electrolyte Solutions. Since the size of the electrolyte drop was larger than the

hanging mercury drop, we started by using a macrophotographic pendant drop method to measure the interfacial tension of the ITIES. This approach was found to be cumbersome and tedious. It was also found to be lacking in accuracy, due not only to the manual single plane measurement[5] but also to the unavoidable deformation of the film during development. We made use, then, of the facility of video image processing offered by the Department of Electronics, with which we developed a method of measuring boundary tension by a new Drop Image Processing method (DIP)[26] . This technique is described in Annexe I. After the satisfactory results obtained from this first approach, it was decided to design a new instrument, solely dedicated to the extraction of the profile coordinates of a pendant drop. This new equipment, called the " line by line digitiser " , was built by Dr. B.D.V. Smith, from the Department of Electronics, with the following features:

a) It extracted the edge coordinates of a pendant drop video image. (ca. 1000 pairs (X,Y) per image).

b) It then displayed the extracted coordinates in the video monitor.

c) It allowed the automatic elimination of the central bright area of the drop caused by lens effects.

d) Finally, the data acquisition time was 40 ms.

With this new type of drop profile data acquisition, it became necessary to develop a completely new computational method capable of processing 1000 pairs of coordinates (X,Y) in a reasonable time.

The development of the line by line digitiser and also the computational method are presented in Part I of this dissertation.

Part II and Part III describe two experiments carried out using this method of measurement of the boundary tension.

The first experiment is a study of the ion free or compact layer between an aqueous solution and an organic phase. Some conclusions, regarding the structure of the interface, are drawn. The second experiment illustrates the possible use of the system in studying the kinetics of adsorption.

Finally, Part IV shows the kind of experiments that can be carried out in the years to come with improvement of the processor capacity.

PART I

CHAPTER 2

THEORY OF MEASUREMENT OF BOUNDARY TENSION FROM LINE BY LINE DIGITISED VIDEO IMAGE OF A PENDANT DROP

2.1. Mathematical basis

2.1.1. Historical development

The possibility of calculating liquid boundary tensions from pendant drop shapes has been considered as early as 1881 by Worthington[72]. The first practical studies were achieved in 1937 by Andreas et al[5] . These authors revised the mathematical theory of the shape of the static drop and developed the method of the selected plane, for which the first empirical tables were derived. Fordham[14] in 1948 and Stauffer[64] in 1965 published computed tables, which allow the use of this method over a wide variety of drop shapes.

2.1.2. Mathematical equations

The mathematical treatment is based on two equations:

- the Laplace equation
- the equation describing the balance between all vertical forces across any horizontal plane of a pendant drop.

These two equations may be combined and solved for γ in many ways. Andreas and Hauser[5] proposed two methods, viz the method of the plane of inflexion and the method of a selected plane. The latter was used in an adapted form in an earlier work, as described in Annexe I. In this chapter, the use of the method of the plane of inflexion from a video drop image digitised line by line, is described.

2.1.2.1. Laplace equation

For a liquid surface to be curved, the pressure on the concave side must be greater than that on the convex side by an amount which depends on the interfacial tension and on the curvature.

If we consider the displacement of a curved surface parallel to itself, the work done to increase the volume of the concave side (as the surface moves towards the convex side), must be compensated by the work done to increase the area. Let a rectangular elementary surface of a curved fluid-liquid interface be in equilibrium, we then have a pressure P outside and a pressure P+ΔP inside, as shown in figure 2.1 .

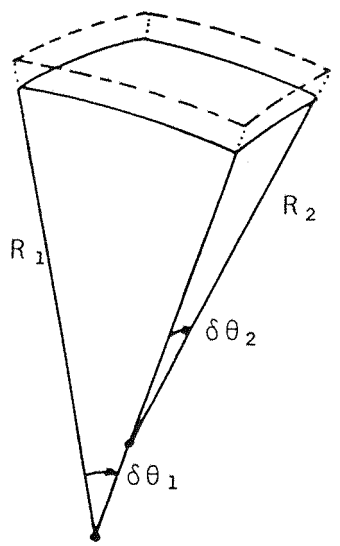

Figure 2.1

The two principle radii of curvature are R_1 and R_2 and the sides of the element substend small angles $\delta\theta_1$ and $\delta\theta_2$, so that the area of the element is

$$R_1\delta\theta_1 R_2\delta\theta_2 \quad .$$

If the surface is moved a small distance δr outwards along its normal, the net work done by the pressure is

$$\Delta P R_1\delta\theta_1 R_2\delta\theta_2\delta r \quad .$$

This balances the other work done, i.e. the product of the increase in area by the surface energy per unit area, which is numerically equal, for the fluid-liquid interface, to the boundary tension γ.

After expansion of the elementary surface the area becomes

$$(R_1+\delta r)\ \delta\theta_1\ (R_2+\delta r)\ \delta\theta_2 \quad ,$$

which, if we neglect the second order term

$$\delta r^2\ \delta\theta_1\delta\theta_2 \quad ,$$

represents an increase of area equal to

$$(R_1+R_2)\ \delta\theta_1\delta\theta_2\delta r \quad .$$

Then, we may write the work balance equation as

$$\Delta P \times R_1R_2\delta\theta_1\delta\theta_2\delta r = \gamma \times (R_1+R_2)\ \delta\theta_1\delta\theta_2\delta r \quad , \qquad (2.1)$$

which is equivalent to

$$\Delta P = \gamma\ (\ 1/R_1 + 1/R_2\ ) \quad . \qquad (2.2)$$

Equation (2.2) is the fundamental equation of Capillarity, and is also called the Laplace equation.

2.1.2.2. Local forces balance

A drop is considered to be in mechanical equilibrium if, at any horizontal plane all vertical forces are balanced. For a pendant drop hanging downwards we have at any horizontal plane P two forces as shown in figure 2.2.

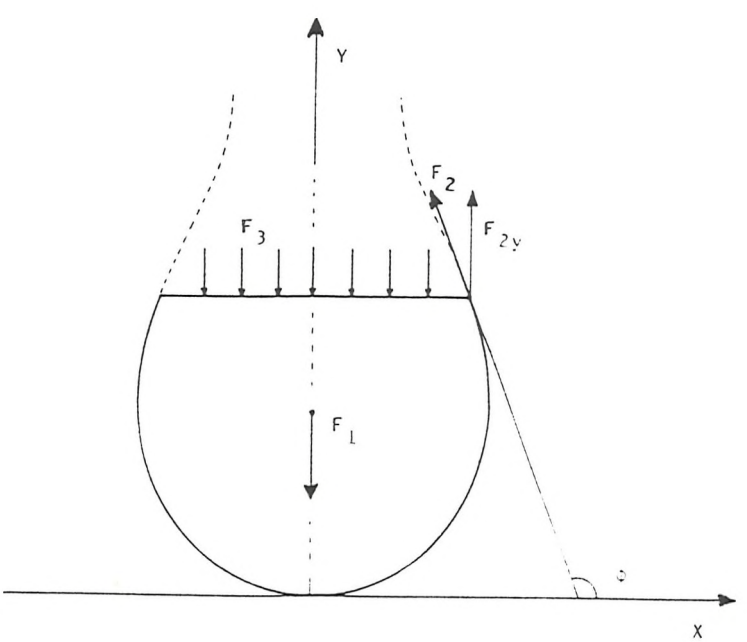

Figure 2.2

F_1, the force of gravity acting downwards, is equal to the weight of the volume of fluid hanging from the plane considered:

$$F_1 = V\sigma g \quad , \tag{2.3}$$

where: V = Volume of fluid hanging under the plane P;
σ = Difference of density between the liquid and the fluid.

The force F_2, is the boundary tension which acts parallel to the boundary. Its projection on the vertical axis, F_{2y}, is upwards and is given by

$$F_{2y} = 2\pi X \times \gamma \times \sin\phi \quad , \tag{2.4}$$

where: γ = Boundary tension;
ϕ = Angle between the tangent and the axis;
X = Cross-sectional radius at the plane P.

Since the volume is in equilibrium, these forces must be balanced by the excess of pressure acting on the plane. It results in a downwards force, F_3, where

$$F_3 = \Delta P \times \pi X^2 \quad , \tag{2.5}$$

with

$$\Delta P = \gamma \left(1/\rho + 1/R \right) \tag{2.6}$$

and: X = Cross-sectional radius at the plane P;
ρ = Internal radius of curvature

$$\rho = ds/d\phi \quad ;$$

R = External radius of curvature

$$R = X/\sin\phi \quad .$$

The local forces balance is then given by the relation

$$F_{2y} = F_1 + F_3 \quad . \tag{2.7}$$

By substituting the equations (2.3),(2.4),(2.5) and (2.6) into equation (2.7) we have

$$2\pi X \gamma \sin\phi = V\sigma g + \pi X^2 \gamma \left(1/\rho + 1/R \right) \quad . \tag{2.8}$$

This equation relates the boundary tension to the geometrical dimensions of the drop and can be used in

many ways for the calculation of boundary tension from drop profile measurements.

2.1.2.3. Method of the selected plane

This method is based on the transformation of equation (2.8) into a system of three first order differential equations with two parameters. This transformation starts with the definition of a parameter b, set to be equal to the common value of the two principal radii of the curvature at the apex of the drop.

$$\rho_{apex} = R_{apex} = b \quad . \qquad (2.9)$$

The parameter b was called in an earlier work (see Annexe 1) the " size parameter " because it is strongly dependent on the size of the drop. The pressure due to the curvature at any plane located at a distance Y from the apex can be given as a function of b and Y by

$$\Delta P = 2\gamma/b - g\sigma Y = \gamma (1/\rho + 1/R) \quad . \qquad (2.10)$$

If we express the external radius of curvature as a function of X and $\sin\phi$, i.e.

$$R = X/\sin\phi \quad ,$$

we have

$$1/\rho + \sin\phi/X = 2/b + \beta Y \qquad (2.11)$$

with β, called in an earlier work the " shape parameter ", equal to

$$\beta = - g\sigma b^2/\gamma \quad . \qquad (2.12)$$

Equation (2.11) is known as the Bashfort and Adams[6] equation. Figure (2.3) and (2.4) show the influence of the parameters b and β on the shape and on the size of pendant drops.

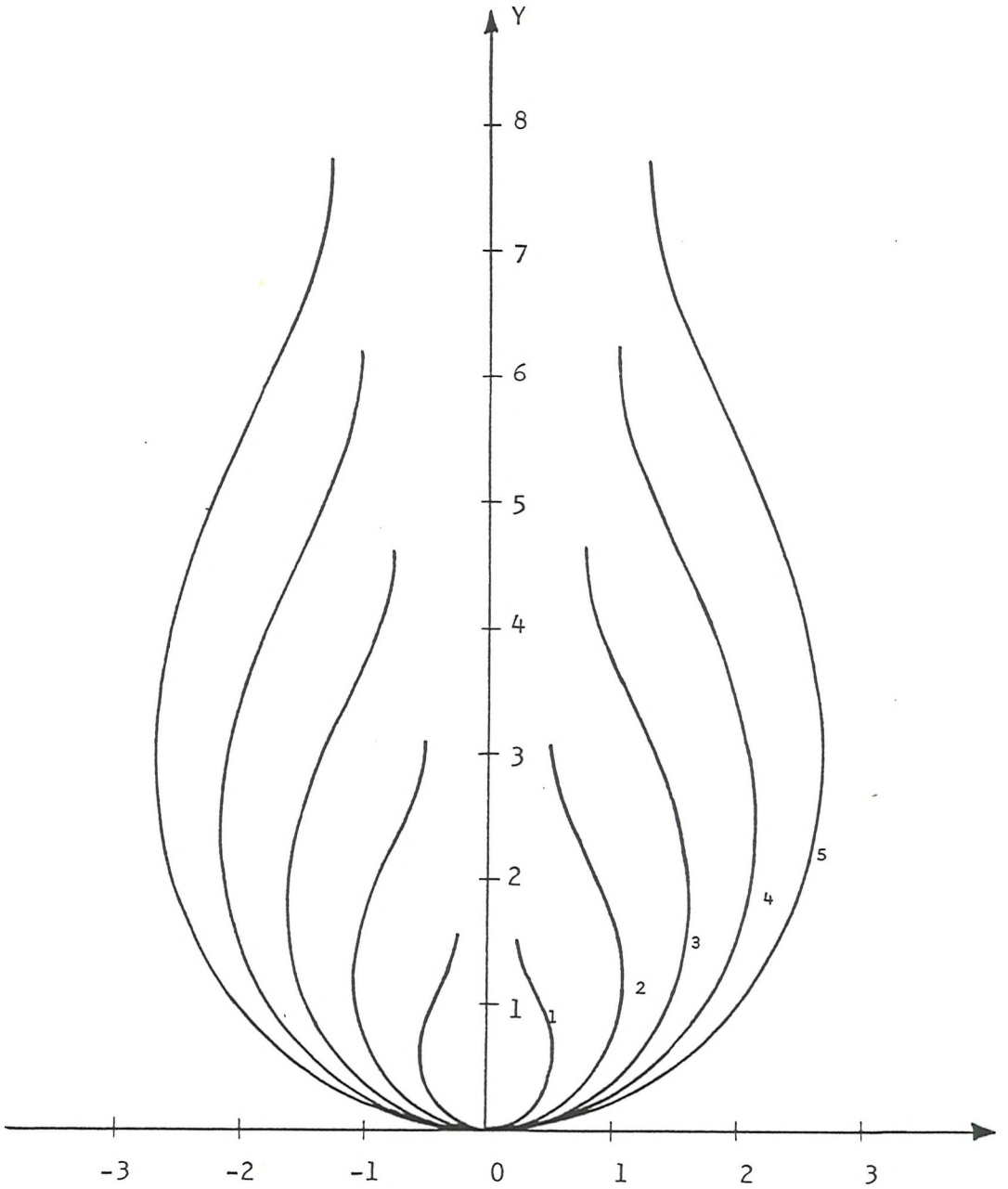

Figure 2.3: Influence of the parameter b on the size of the drop

(β = 0.35 = Cst)

(1) : b = 0.5
(2) : b = 1.0
(3) : b = 1.5
(4) : b = 2.0
(5) : b = 2.5

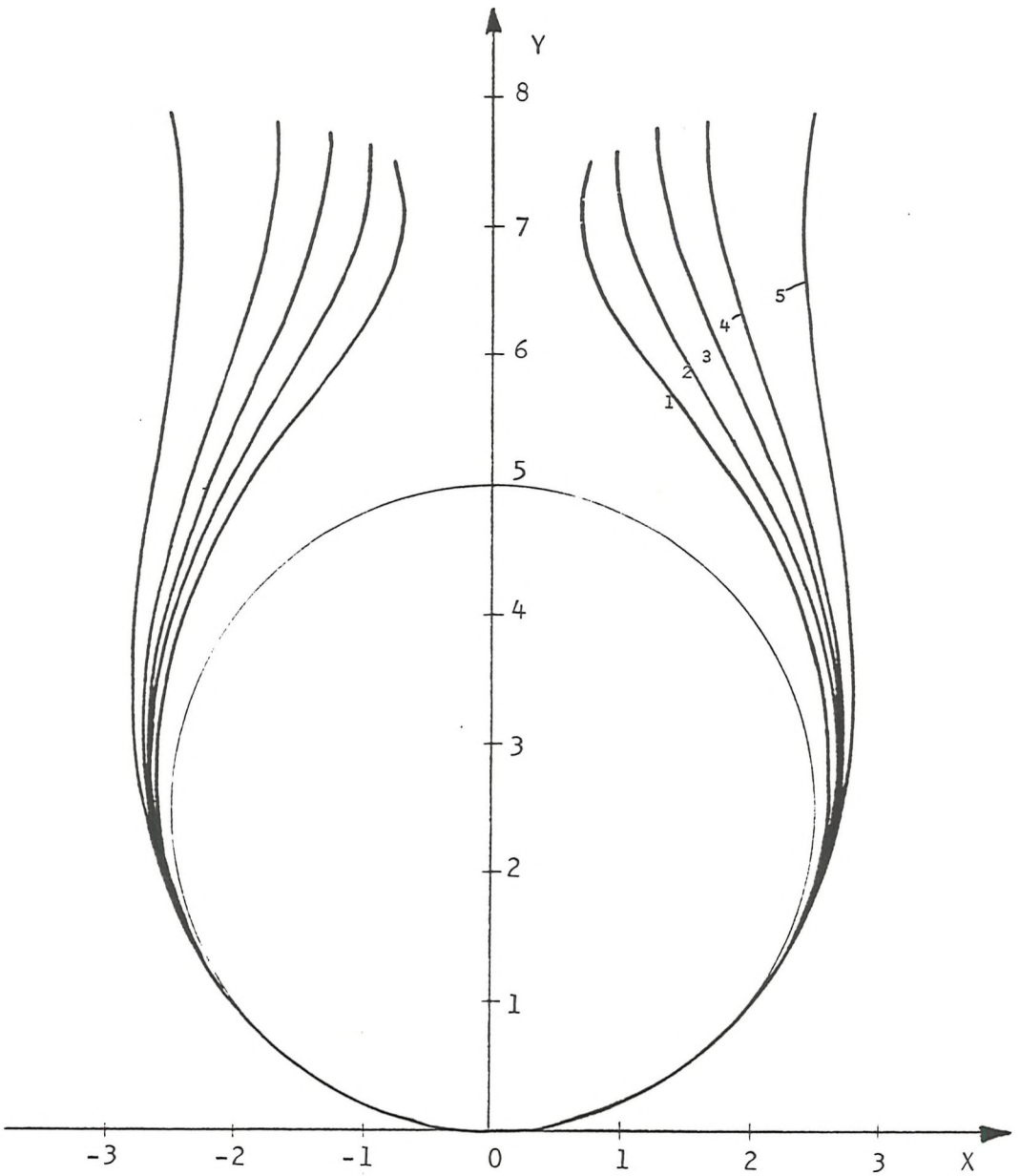

Figure 2.4: Influence of the parameter β on the shape of a pendant drop

(b = 0.25 = Cst)

(1) : β = 0.25
(2) : β = 0.30
(3) : β = 0.35
(4) : β = 0.40
(5) : β = 0.50

Since ρ is the internal radius of curvature,

$$\rho = \frac{ds}{d\phi} \quad ,$$

equation (2.11) can be recast in the form of a system of three first order differential equations:

$$dX = \cos\phi \, ds \tag{2.13}$$

$$dY = \sin\phi \, ds \tag{2.14}$$

$$d\phi = \left(\frac{2}{b} + \beta Y - \frac{\sin\phi}{X} \right) ds \tag{2.15}$$

This system was first solved by S. Fordham[14] using numerical integration techniques, and later by C.E. Stauffer[64] over a wider range of the parameter β. The method of the selected plane involves the determination of the two parameters, b and β, by measuring the equatorial diameter of the drop, de, and the diameter, ds, at a selected plane located at a distance, de, from the apex. Using tables, it is possible to deduce the value of the boundary tension from these two measurements. In an earlier work this method was employed using about 100 selected planes per drop, as described in Annexe 1.

The computational method of calculation was based on the study of the respective influence of the parameters b and β on the root mean square residual of the fitting of the 100 data points to the drop profiles generated by solving equations (2.13), (2.14) and (2.15). The resolution of this system was done using a Runge-Kutta integration technique. It was observed that b and β could be optimized independently of each other using a successive approximation approach. This sequential approximation could be done because it had been observed that a plot of the root mean square residual as a function of the parameters, b and β, results in a set of curves as shown in figure 2.5.

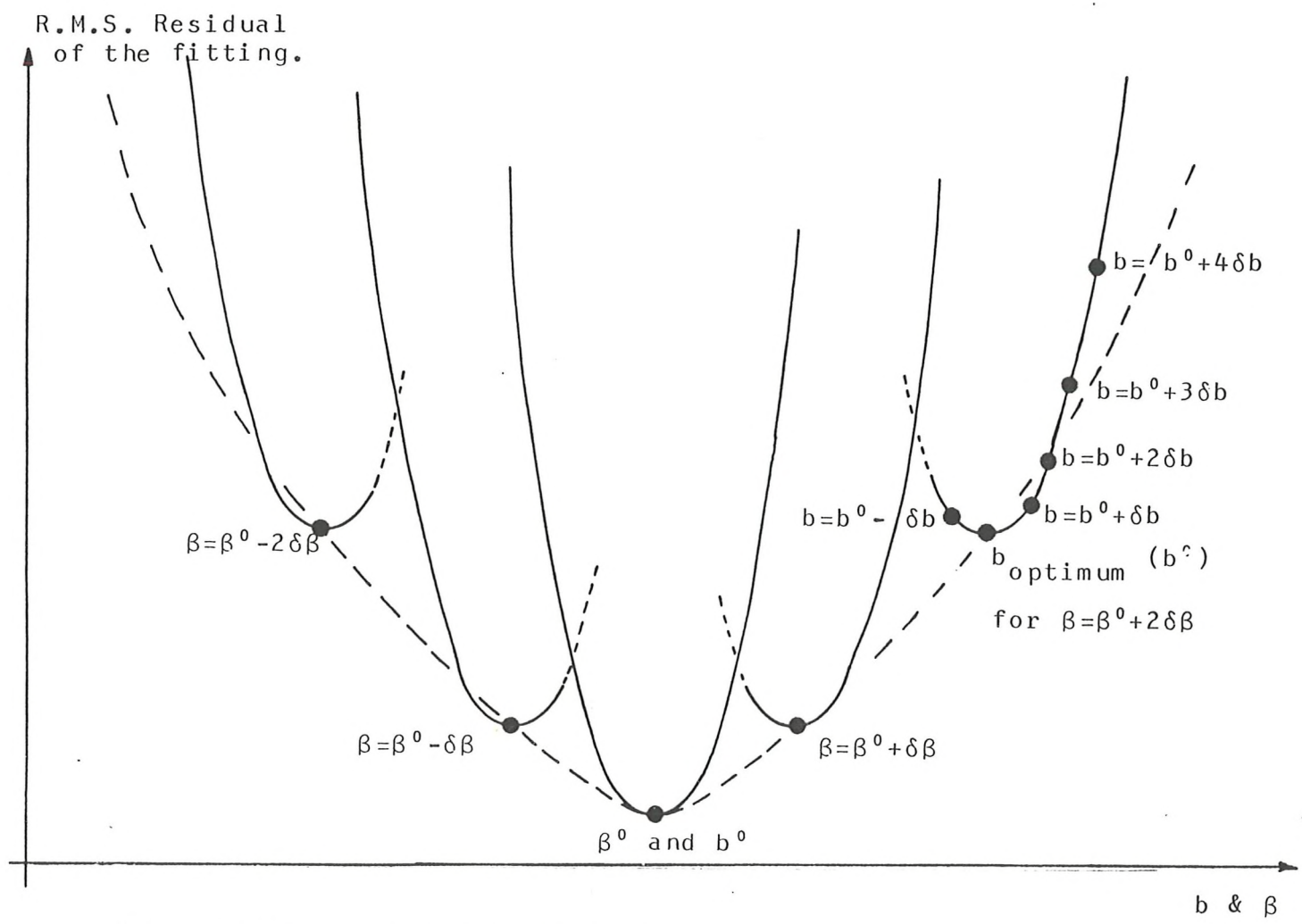

Figure 2.5: Optimisation of the parameters b and β by sequential determination of the minimum of the R.M.S. residual of the polynomial fitting.

The optimal values of b and β were those for which the R.M.S. residual was minimal. The accuracy of this determination was a function only of the length of the step of approximation used during the final approach.

The method was very accurate because it involved performing a signal averaging process with 100 selected planes instead of the two usually considered planes in the classical pendant drop treatment. With the development of a new line by line digitiser, designed to increase the speed of data acquisition, the number of selected planes measured was about 500.

As the computational time needed for 100 selected planes was already long (ca. 20 minutes) the time required for 500 selected planes made the method completly inadequate. Thus a new method of analysis had to be developed.

2.1.2.4. Method of the inflexion plane

For a drop formed on a capillary tip, (the size of the drop being large in comparison with the tip), a "neck", or change of curvature, is formed between the tip and the equatorial diameter of the drop. For this type of drop, equation (2.8) can be solved at the inflexion plane by a mathematically exact solution.

Indeed, at the inflexion plane, the external radius of curvature ρ is infinite, and therefore the Laplace equation is reduced to

$$\Delta P = \gamma/R \quad . \qquad (2.16)$$

Substituing equation (2.16) into equation (2.8), the boundary tension can be expressed by

$$\gamma = \frac{V\sigma g}{2\pi X \sin\phi - \pi X^2/R} \qquad (2.17)$$

If we replace the value of R in equation (2.17) by the

by the expression

$$R = \frac{X}{\sin\phi} \quad ,$$

we obtain, for the special case where ρ is infinite,

$$\gamma = \frac{V\sigma g}{\pi X \sin\phi} \quad . \qquad (2.18)$$

This solution has the advantage of being mathematically exact. The difficulty of this method lies in the determination of the location of the inflexion plane and also in the calculation of the volume of the drop beneath this plane. This determination is very difficult graphically. However, the development of image processing and especially the development of a line by line video digitiser has circumvented this difficulty.

The second part of this chapter describes the computational technique used to locate the inflexion plane of a drop from its video digitised image.

2.2. Computational method

2.2.1. Introduction

The computational method described in this chapter has been developed especially for use with a line by line video image digitiser. The description of the functions of the hardware and software used for the data acquisition is given in chapter 3, together with the data presentation.

The data after acquisition is processed in order to be presented as a set of (X_i, Y_i) coordinates of about 1000 points. These coordinates are classified in the following way:

$$\begin{array}{cc} (X_{L1}, Y_1) & (X_{T1}, Y_1) \\ (X_{L2}, Y_2) & (X_{T2}, Y_2) \\ \vdots & \vdots \\ (X_{L500}, Y_{500}) & (X_{T500}, Y_{500}) \end{array} ,$$

where X_{Li} represents the coordinate of the leading edge of the i^{th} line, and X_{Ti} the coordinate of the trailing one. The system of coordinates is centered, for pendant drops hanging downwards and upwards, as shown in figure 2.6 and 2.7 respectively.

The values of X_i are expressed in pixel units (1066 pixels per video line) and the values of Y_i are expressed in line units (575 working video lines per frame). The coordinates (X_i, Y_i) give therefore a staircase representation of a drop image and will be processed as such.

The computational method consists in the calculation of equation (2.18) by determination of the inflexion plane followed by:

a) the calculation of the cross-sectional radius at this plane X_{inf},

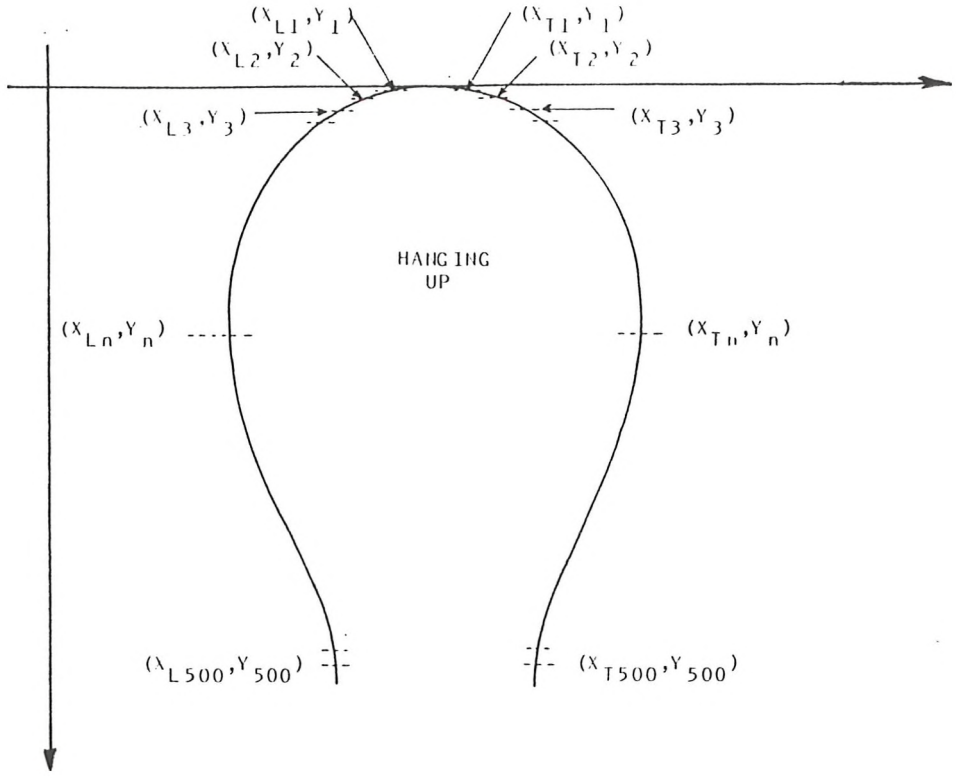

Figure 2.5: X,Y coordinates of a pendant drop given by the digitiser

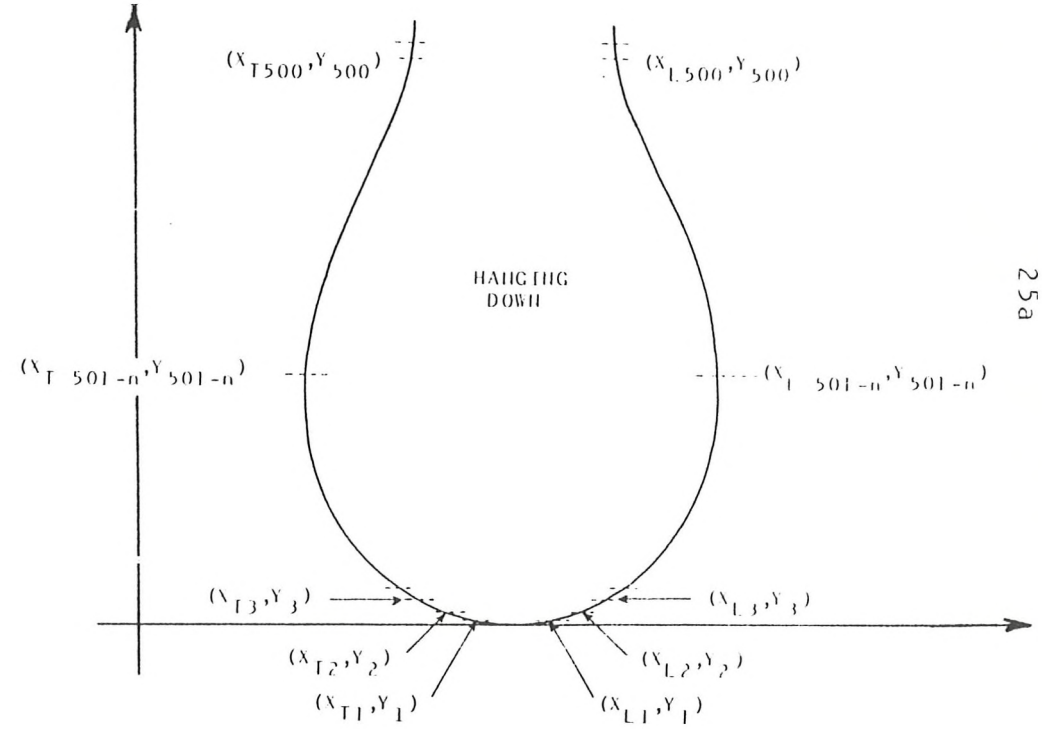

Figure 2.6: X,Y coordinates of a pendant drop after classification of the data points.

b) the sine of the angle ϕ at this plane, $\sin\phi_{inf}$, and

c) the volume V of fluid hanging beneath the plane.

2.2.2. Determination of the inflexion plane

2.2.2.1. Curve - fitting techniques

Given a set of data points (X_i, Y_i) forming a staircase shape representation of a function

$$Y_i = f(X_i) \quad ,$$

the common way to identify the plane of inflexion of this function f is to use a curve - fitting technique in order to obtain a polynomial representation

$$Y_i = P(X_i) \quad .$$

The position of the plane of inflexion is then found by solving equation (2.19) for X, i.e.

$$P''(X) = 0 \qquad (2.19)$$

This technique is more appropriate to a staircase data series than a differentiation technique based on the Taylor series using the nearest neighbours. Furthermore, in the present case, the advantage of the curve - fitting technique is not only that it smooths the staircase, but also it considers a greater number of coordinates (about 500 points) instead of only twenty nearest neighbours. The resulting smoothing of so many data points is somewhat similar to a signal averaging of the coordinates.

Three main polynomial curve - fitting techniques are available:

a) the Chebyshev minimax polynomial fit where the function

$$\text{Max} \left(P(X_i) - Y_i \right) \quad \text{or} \quad \sum_{i=1}^{n} P(X_i) - Y_i$$

is minimized;

b) the least square polynomial approximation where the root mean square residual

$$\sqrt{\sum_{i=1}^{n} \left(P(X_i) - Y_i \right)^2}$$

is minimized;

c) the cubic spline polynomial fit where the function to be minimized is

$$\int_a^b \left(f^{(q)}(X) \right)^2 dX$$

The method of minimax polynomial fit is not really appropriate for the determination of the inflexion point of a curve. The reason for this is that the change of curvature around the inflexion point can alter the sign of the expression

$$P(X_i) - Y_i \quad ,$$

which can involve an error in the minimization, leading to a false approximation.

The cubic spline approximation is by its nature un - suitable for a staircase - shape set of data points, because in this case, the "knots" of the splines are not known accurately. Furthermore, the processing of about 250 pairs of coordinates (X_i, Y_i) would involve 250 coefficients in the spline, i.e.

$$P(X) \equiv C_1 N_1(X) + C_2 N_2(X) + \ldots\ldots + C_{250} N_{250}(X) \quad ,$$

where $N_i(X)$ is the normalized cubic B-spline. These two reasons make this method completly inadequate in the present case.

The least square polynomial curve - fitting is, however, quite well suited for our purpose. This method can approximate a polynomial to as many data points as required and does not present any error in the determination of an inflexion point. Also, the influence of parasite "wild"

points is attenuated compared with the two other methods. Furthermore, this technique is computationally fast and provides more information on which to assess the results. The relatively small size of the memory arrays required makes this method very appropriate for use on small computers like the Digital LSI 11/23. For practical computational purposes, the polynomial is expressed in its Chebyshev series form

$$P(X) \equiv \frac{1}{2} A_0 T_0(x) + A_1 T_1(x) + \ldots\ldots + A_n T_n(x) \quad ,$$

where $T_i(x)$ is the Chebyshev polynomial of the first kind of degree i, where the range of X has been normalized to run from -1 to +1 in the following way:

$$x = \frac{(X - X_{min}) - (X_{max} - X)}{X_{max} - X_{min}} \quad .$$

This form is usually preferred to the power series

$$P(X) \equiv a_0 + a_1 X + a_2 X^2 + \ldots\ldots + a_n X^n$$

since it leads to a higher accuracy, both in the computation of the coefficients and the subsequent evaluation of the fitted polynomial at specified points.

All the subroutines used during the development of this method were adapted from the N.A.G. library.

2.2.2.2. Least square approximation of the drop profile

The computational method used for the least square fitting of a polynomial

$$Y = P(X)$$

from a set of points (X,Y) requires that the points be ordered in increasing values of X. In our case the (X_i, Y_i) coordinates of the drop profile were classified by increasing values of Y_i, as shown in figure 2.6 and 2.7.

Therefore it was logical to fit a polynomial P as a function of Y_i,

$$X_i = P(Y_i) \quad .$$

The least square approximation $P(Y_i)$ was restricted to the points located between the equator of the drop and the capillary. The reason for this choice was that the computational time necessary for the evaluation of the polynomial was proportional to the number of data points considered. Also, in this part of the drop profile the change of curvature was limited compared to the spherical apex of the drop and therefore, the quality of the fitting was better.

There were two ways by which the drop profile could be approximated to a polynomial:

a) The first way was to use only the points located on one side of the drop. It was then possible either to fit a polynomial P_L defined by equation (2.20)

$$X_{Li} = P_L(Y_i) \qquad (2.20)$$

where X_{Li} is the coordinate of the leading edge of the i^{th} line, or to fit a polynomial P_T defined by equation (2.21)

$$X_{Ti} = P_T(Y_i) \qquad (2.21)$$

where X_{Ti} is the coordinate of the trailing edge of the i^{th} line. The location of the inflexion plane was then calculated for each side and the average was taken as a final value. It was observed that for a polynomial greater or equal to 3, the root mean square residual,

$$\sqrt{\sum_{i=1}^{n} \left(X_i - P(Y_i) \right)^2} \quad ,$$

was more or less constant with a value between 0.3 and 0.5 pixels. This was due to the fact that we tried to approximate a staircase - shape function by a polynomial.

b) A second possibility was to fit a polynomial P_Δ defined by equation (2.22)

$$\Delta X_i = X_{Ti} - X_{Li} = P_\Delta(Y_i) \qquad (2.22)$$

where ΔX_i represents the cross-sectional diameter of the drop in the i^{th} line. In this particular case, the location of the inflexion plane was also calculated by solving equation (2.23) for Y.

$$P''_\Delta(Y_i) = 0 \qquad (2.23)$$

As for the first approximation it was observed that, here too, for a polynomial P_Δ of a degree greater or equal to 3, the R.M.S. residual

$$\sqrt{\sum_{i=1}^{n} \left(\Delta X_i - P_\Delta(Y_i) \right)^2}$$

was constant, with a value between 0.5 and 0.9 pixels.

The second method of drop profile approximation was chosen because it considered both sides of the drop in the same computational time as was necessary for the curve - fitting of 250 data points. The degree of polynomial used was 3 as this degree combines an adequate approximation with a good smoothing of the staircase representation of the drop. The use of higher degrees did not improve the R.M.S. residual, and furthermore, they only increased the computational time.

2.2.2.3. Location of the inflexion plane

The distance Y_{inf} between the inflexion plane and the apex of the drop was calculated by solving equation (2.23) from the polynomial expression, $P_\Delta(Y_i)$, i.e.

$$P_{\Delta}(Y_i) = 0.5\, A_0 T_0(y_i) + A_1 T_1(y_i) + A_2 T_2(y_i) + A_3 T_3(y_i)$$

where y_i is the normalized value of Y_i (as given by equation (2.24)), i.e.

$$y_i = \frac{(Y_i - Y_1) - (Y_N - Y_i)}{(Y_N - Y_1)} \qquad (2.24)$$

with Y_1 and Y_N being respectively the smallest and the largest value of Y_i. The second derivative of the polynomial P_{Δ} was first calculated in its power series form and the solution of equation (2.23) was given by

$$Y_{inf} = \frac{1}{2}\left(\left(\frac{A_2}{6A_3} \right) (Y_N - Y_1) + Y_1 + Y_N \right) \qquad (2.25)$$

2.2.3. Calculation of X_{inf} and $\sin\phi_{inf}$

The value of the cross-sectional radius at the inflexion plane, X_{inf}, is given by equation (2.26)

$$X_{inf} = \frac{1}{2}\Delta X_{inf} = \frac{P_{\Delta}(Y_{inf})}{2} \qquad (2.26)$$

The calculation of $P_{\Delta}(Y_{inf})$ was done by the following recurrences:

a) Gentleman's modified recurrence for $-1 < y_{inf} < -0.5$ [73]

b) Clenshaw's original recurrence for $-0.5 < y_{inf} < 0.5$ [74]

c) Reinch's modified recurrence for $0.5 < y_{inf} < 1$ [73]

where y_{inf} is the normalized value of Y_{inf}.

The subroutine used for the calculation of $P_{\Delta}(Y_{inf})$ was adapted from the N.A.G. library.

The value of the angle ϕ was found by calculation of the slope of the tangent at the inflexion plane as given by equation (2.27)

$$tg\phi_{inf} = \frac{P'_{\Delta}(Y_{inf})}{2} \qquad (2.27)$$

$P'_{\Delta}(Y_{inf})$ was worked out using equation (2.28)

$$P'_{\Delta}(Y_{inf}) = (Y_N - Y_1)\ (\ A_1 + 4A_3 \cdot y_{inf} + A_4 \cdot\ (12y_{inf} - 3)\ ). \qquad (2.28)$$

The sine of the angle ϕ_{inf} was calculated from the library functions SINE and ARCTANGENT provided by FORTRAN IV.

2.2.4. Calculation of the volume hanging from the inflexion plane

The method adapted to calculate the volume between the apex and the plane of inflexion was a Riemann integration technique since the drop profile of the digitised drop image was in the form of a staircase function. This was equivalent to calculating the volume of a stack of discs, each disc having a diameter ΔX_i and a thickness h, equal to the distance between two video lines. Therefore, if Y_I is the integer truncation of Y_{inf}, the volume is given by

$$V = \sum_{i=1}^{I} \frac{h\pi}{4} \Delta X_i^2 \qquad (2.29)$$

Equation (2.29) is the Riemann representation of the true volume, which is

$$V = \int_0^{Y_{inf}} \frac{\pi}{4}\ \Delta X^2(y)\ \ dy \qquad (2.30)$$

where $X(y)$ is the cross-sectional diameter at a plane located a distance y from the apex of the drop.

The main advantages of this method was its simplicity and therefore, its short computational time.

2.2.5. Calculation the boundary tension

After having calculated X_{inf}, $\sin\phi_{inf}$ and V, it is possible to calculate the interfacial tensions from equation (2.18)

$$\gamma = \frac{V \sigma g}{\pi X_{inf} \sin\phi_{inf}} \qquad (2.18)$$

the ratio $\gamma/\sigma g$ is given by

$$\frac{\gamma}{\sigma g} = \frac{V}{\pi X_{inf} \sin\phi_{inf}} \quad . \qquad (2.31)$$

As we have seen in sections 2.2.3. and 2.2.4. all the calculations were carried out using the units provided by the line by line digitiser which are:

number of lines for the vertical axis and

number of pixels for the horizontal axis.

The ratio $\gamma/\sigma g$ given by equation (2.31) is then expressed in units of

$$\frac{\gamma}{\sigma g} \simeq \frac{\text{Pixel}^2 \quad \text{line}}{\text{Pixel}}$$

In order to calculate the boundary tension in SI units it is therefore necessary to convert the digitiser output into

metric units. This conversion was performed by calibration as fully described in paragraph 3.4.

Since the ratio between pixel units and line units is a constant of the camera used, the vertical dimension as a function of the horizontal dimension was expressed by introducing a factor called ECHELL (cf. 3.4.1.), which is the number of lines per pixel and was found in our case to be equal to:

$$ECHELL = 0.6784 \text{ lines/pixel} .$$

The conversion of the horizontal dimension into metric units was carried out for each ratio of reproduction used by introducing a factor called SCALE expressed as a number of pixels per mm (cf. § 3.4.2.). From these two factors, it was possible to calculate the ratio $\gamma/\sigma g$ in metric units (mm^2) by multiplying the value obtained from equation (2.31) by a conversion factor equal to

$$\frac{1}{ECHELL \times SCALE^2} .$$

The final value of the boundary tension was then calculated from equation (2.18) expressing the density difference in 10^3 kg $\cdot$ m^{-3} and the gravity acceleration in N $\cdot$ kg^{-1} (g = 9.81422 in Southampton). The resulting boundary tension value is then expressed in mN $\cdot$ m^{-1} .

2.3. Evaluation of the error of the method

2.3.1. Method of analysis

The evaluation of the error in the method is a very delicate exercise. Nevertheless, this section describes an approach of this evaluation based on qualitative arguments and observations. As seen in § 2.1.2.4., the boundary tension is calculated by equation (2.18).

$$\gamma = \frac{V \sigma g}{\pi X_{inf} \sin\phi_{inf}} \qquad (2.18)$$

Except for σ and g, none of the parameters of this equation is an independent variable. Indeed, they are all linked to the determination of the plane of inflexion, which is itself calculated from the measurement of ΔX_i for each video line. The general equation for the error in boundary tension is given by

$$\frac{d\gamma}{\gamma} = \frac{dV}{V} + \frac{dX_{inf}}{X_{inf}} + \frac{d\sin\phi_{inf}}{\sin\phi_{inf}} \qquad (2.33)$$

2.3.2. Calculation of dX_{inf}/X_{inf}

Since the calculation of X_{inf} is based only on the measurement of ΔX_i, one can write

$$dX_{inf} = \frac{\partial X_{inf}}{\partial \Delta X_i} d\Delta X_i \qquad (2.34)$$

where $d\Delta X_i$ is the error in the variable ΔX_i and dX_{inf} the error on X_{inf}. We could carry out the calculation stating that

$$X_{inf} = 1/2\ P_{\Delta}(Y_{inf}) \quad ,$$

but at the end of the derivation we would have to calculate the quantities

$$\frac{\partial a_i}{\partial \Delta X_i}$$

for each value of i, where a_i is the coefficient of the third order polynomial P_Δ. Unfortunately, this calculation is very difficult.

Another approach is to evaluate directly the quantity dX_{inf}/X_{inf} from the results obtained during this work. Two examples of this evaluation are presented from the data given for minimum and maximum values of the angle ϕ (75^0 and 80^0) respectively, in Table 2.1 and Table 2.2 .

These tables show the variation of the different parameters Y_i, ΔX_i, $P(X_i)$ for $i = I \pm 5$, where I is the index of the video line located just under the plane of inflexion. The values of ϕ, V and γ given in the tables are calculated by considering the planes located at a distance Y_i from the apex as the inflexion planes. We can see from these two tables that $\delta P(Y_i)/P(Y_i)$ is constant in this part of the drop and is smaller than 0.15 % between two consecutive lines. Therefore, if we estimate for example the accuracy of the location of the inflexion plane to one video line

$$Y_{inf} = Y_{inf} \pm 1 \quad ,$$

we can calculate, from equation (2.26), the error on X_{inf} by

$$\frac{d X_{inf}}{X_{inf}} = \frac{1}{2} \cdot \frac{d P(Y_{inf})}{P(Y_{inf})} = 0.08 \ \%$$

or

$$\frac{d X_{inf}}{X_{inf}} < 0.1 \ \% \quad .$$

i	Y_i lines	ΔX_i pixels	$P(Y_i)$ pixels	$\frac{\delta \Delta X_i}{\Delta X_i}$ %	ϕ degrees	V mm^3	$\frac{\delta V}{V}$ %	γ $mN\ m^{-1}$	$\frac{\delta \gamma}{\gamma}$ %
I-5	386	501	501.0067	0.15	$75^{o}825$	113.5	0.26	51.681	0.41
I-4	387	500	500.2619	0.15	75.819	113.8	0.26	51.893	0.40
I-3	388	499	499.5168	0.15	75.814	114.1	0.26	52.104	0.40
I-2	389	498	498.7716	0.15	75.811	114.4	0.26	52.315	0.40
I-1	390	499	498.0261	0.15	75.809	114.7	0.26	52.528	0.40
I	391	496	497.2806	0.15	75.808	115.0	0.26	52.739	0.40
I+1	392	496	496.5351	0.15	75.808	115.3	0.26	52.950	0.40
I+2	393	496	495.7896	0.15	75.809	115.6	0.26	53.162	0.40
I+3	394	494	495.0441	0.15	75.812	115.9	0.26	53.373	0.40
I+4	395	494	494.2989	0.15	75.815	116.1	0.26	53.584	0.40
I+5	396	493	493.5538		75.820	116.4		53.795	

Table 2.1 System: LiCℓ (1.462 Molar) / n-Heptane;
R.M.S. residual of the polynomial fitting = 0.87316;
External diameter of the capillary = 7 mm;
Calibration: SCALE = 99.65 pixel · mm^{-1}.

i	Y_i lines	ΔX_i pixels	$P(Y_i)$ pixels	$\frac{\delta \Delta X_i}{\Delta X_i}$ %	ϕ degrees	V mm^3	$\frac{\delta V}{V}$ %	γ $mN\ m^{-1}$	$\frac{\delta \gamma}{\gamma}$ %
I-5	365	548	548.1955	0.08	81^o657	110.6	0.32	26.814	0.40
I-4	366	548	547.7631	0.08	81^o653	111.0	0.32	26.921	0.40
I-3	367	547	547.3304	0.08	81^o649	111.3	0.32	27.027	0.40
I-2	368	547	546.8975	0.08	81^o646	111.7	0.32	27.139	0.40
I-1	369	547	546.4645	0.08	81^o644	112.0	0.32	27.241	0.40
I	370	545	546.0315	0.08	81^o643	112.4	0.32	27.347	0.40
I+1	371	545	545.5984	0.08	81^o643	112.7	0.32	27.453	0.40
I+2	372	545	545.1653	0.08	81^o643	113.0	0.32	27.560	0.40
I+3	373	545	544.7323	0.08	81^o645	113.4	0.32	27.666	0.40
I+4	374	544	544.2993	0.08	81^o647	113.7	0.32	27.773	0.40
I+5	375	544	543.8666		81^o651	114.1		27.879	

Table 2.2 System: KCℓ (0.579 Molar) / 1,2-dichlorethane;
R.M.S. residual of the polynomial fitting = 0.76343;
External diameter of the capillary = 5 mm;
Calibration: SCALE = 99.65 pixel • mm^{-1}.

2.3.3. Calculation of $d\sin\phi_{inf}/\sin\phi_{inf}$

As in the calculation of dX_{inf}/X_{inf}, it is possible to calculate $d\sin\phi_{inf}/\sin\phi_{inf}$ by stating that

$$\sin\phi_{inf} = \frac{\tan\phi_{inf}}{\sqrt{1 + \tan^2\phi_{inf}}}$$

and then, that

$$d\ \sin\phi_{inf} = \cos^3\phi_{inf} \cdot d\ \tan\phi_{inf} \quad , \qquad (2.35)$$

with

$$d\ \tan\phi_{inf} = d\ P'(Y_{inf}) \quad . \qquad (2.36)$$

But, as for the last case, a full derivation will end in the calculation of the quantities

$$\frac{\partial\ a_i}{\partial \Delta X_i} \quad .$$

Again, another approach is to estimate the error in the calculation of $\sin\phi_{inf}$. It is known that around any point of inflexion the slopes of the tangents are rather similar. Also in the case of the pendant drop the angle ϕ_{inf} lies between 75^0 and 80^0 and thus the sine is nearly equal to 1. Therefore, we may assume that the error $d\phi_{inf}$ is more or less independent of the accuracy of the location of the inflexion plane and, furthermore, that the sine function varies only slightly for angles close to $\pi/2$. Hence, it may be considered that $d\sin\phi_{inf}/\sin\phi_{inf}$ is neglegible. This estimation is confirmed by the results shown in Table 2.1 and Table 2.2 .

2.3.4. Calculation of the error dV/V

We have seen in paragraph § 2.2.4. that the volume V is given by equation (2.29):

$$V = \sum_{i=1}^{I} \frac{h\ \pi}{4} \Delta X_i^2 \quad . \qquad (2.29)$$

This equation is equivalent to

$$V = \int_0^{Y_{inf}} \frac{\pi}{4} \Delta X^2(y)\ dy \qquad (2.30)$$

where $\Delta X(y)$ is the cross-sectional diameter of the drop at a plane located a distance y from the apex. The error made during the calculation of the volume depends on the error made in measuring ΔX and also on the location of the inflexion plane, Y_{inf}. This is given by

$$dV = \frac{\partial V}{\partial \Delta X} d\Delta X + \frac{\partial V}{\partial Y_{inf}} dY_{inf} \quad . \qquad (2.37)$$

The two partial derivatives of the volume can be obtained from equation (2.30) by derivation over ΔX

$$\frac{\partial V}{\partial \Delta X} = \int_0^{Y_{inf}} \frac{\pi}{2} \Delta X(y)\ dy = \frac{A}{2} \ , \qquad (2.38)$$

where A is the area of the drop hanging beneath the inflexion plane, and by derivation over Y_{inf}

$$\frac{\partial V}{\partial Y_{inf}} = \frac{\pi}{4} \Delta X^2{}_{inf} \ . \qquad (2.39)$$

On substituting equations (2.38) and (2.39) into equation (2.37) we obtain

$$dV = \frac{A}{2} d\Delta X + \frac{\pi}{2} \Delta X^2{}_{inf}\ dY_{inf} \quad . \qquad (2.40)$$

The evaluation of $d\Delta X$ in the first term is rather delicate because it involves the estimation of a given curve by a staircase representation. It also involves the estimation of the accuracy of the drop edge extraction by the hardware. The second estimation can be made from the observation of the standard deviation obtained during the calibration of vertical cylinders. Therefore if the first source of error is negligibly small compared with the second one, it is possible to estimate from paragraph § 3.5. $d\Delta X$ to be equal to one pixel.

$$d\Delta X = 1 \text{ pixel} .$$

If we estimate, as in paragraph § 2.3.2., the accuracy of location of the inflexion plane to be equal to one video line

$$dY_{inf} = 1 \text{ line} ,$$

it is possible to evaluate equation (2.40) using for example the values given in Table 2.1 and 2.2 .

From Table 2.1, we can extract the following data:

$$\Delta X_{inf} = 5.48 \text{ mm} \qquad A = 85.55 \text{ mm}^2$$
$$dY_{inf} = 1.5 \cdot 10^{-2} \text{ mm} \qquad V = 112.40 \text{ mm}^3$$
$$d\Delta X = 1 \cdot 10^{-2} \text{ mm}$$

which give

$$dV = 0.428 + 0.354 = 0.782 \text{ mm}^3 ,$$

or

$$\frac{dV}{V} = 0.7 \% .$$

From Table 2.2, we can repeat the calculation with

$$\Delta X_{inf} = 4.99 \text{ mm} \qquad A = 89.25 \text{ mm}^2$$
$$dY_{inf} = 1.5 \cdot 10^{-2} \text{ mm} \qquad V = 115.10 \text{ mm}^3$$
$$d\Delta X = 1 \cdot 10^{-2} \text{ mm} ,$$

then

$$dV = 0.446 + 0.293 = 0.739 \text{ mm}^3,$$

or

$$\frac{dV}{V} = 0.6 \% \quad .$$

Therefore, we can say that

$$\frac{d\,V}{V} < 0.7 \% \quad .$$

2.3.5. Conclusion

Equation (2.33) can now be evaluated

$$\frac{d\,\gamma}{\gamma} = \frac{d\,V}{V} + \frac{dX_{inf}}{X_{inf}} + \frac{d\,\sin\phi_{inf}}{\sin\phi_{inf}} \qquad (2.33)$$

using the values found previously, i.e.

$$\frac{d\,\gamma}{\gamma} = 0.7 \% + 0.1 \% < 1 \% \quad .$$

This represents only the error arising from the calculation of γ and does not take the calibration of the horizontal axis into account. This latter error can be calculated from equation (2.32)

$$\frac{\gamma}{\sigma\, g} = \left(\frac{\gamma}{\sigma\, g} \right) \times \frac{1}{ECHELL \times SCALE^2} \qquad (2.32)$$

by

$$\frac{d\,\gamma}{\gamma} = \frac{d\,\gamma}{\gamma} + \frac{d\,ECHELL}{ECHELL} + 2\,\frac{d\,SCALE}{SCALE} \qquad (2.41)$$

As will be seen later in paragraph § 3.5., the last two terms can be estimated as follows:

$$\frac{d\ SCALE}{SCALE} \simeq 0.2\ \% \qquad \frac{d\ ECHELL}{ECHELL} \simeq 0.5\ \%$$

Therefore, it may be concluded that at a given calibration the error in the method is less than 1 %. For measurements of absolute values where the error of the calibration is taken into account the total error is about 2 % for each individual measurement.

If we compare these estimated values with the experimental results obtained, we can see that they are greater than the standard deviation of the measurements. From experience we can say that at a constant calibration the standard deviation over a set of 100 measurements of a given system (5 drops and 20 measurements per drop) is

$$\frac{d\ \gamma}{\gamma} < 0.5\ \% \quad .$$

On the other hand, if we compare the results obtained for well known systems like water/nitrobenzene and water/n-heptane , our absolute measurements are within 1 % of the values given in the literature. This is a consequence of the averaging of the many automatic sequential measurements performed on each drop.

CHAPTER 3

LINE BY LINE DROP IMAGE DIGITISATION SYSTEM

3.1. Introduction

This chapter will be dedicated to the description of the equipment used in the measurement of the boundary tension from a digitised video drop image. This presentation can be divided in three parts. The first part describes the system necessary to obtain a video image of a fluid drop. The second part explains how this video image is digitised and transferred to a processor with different choices of data acquisition. The final part shows how to calibrate the whole system.

A schematic diagram of the equipment used is given in figure 3.1.

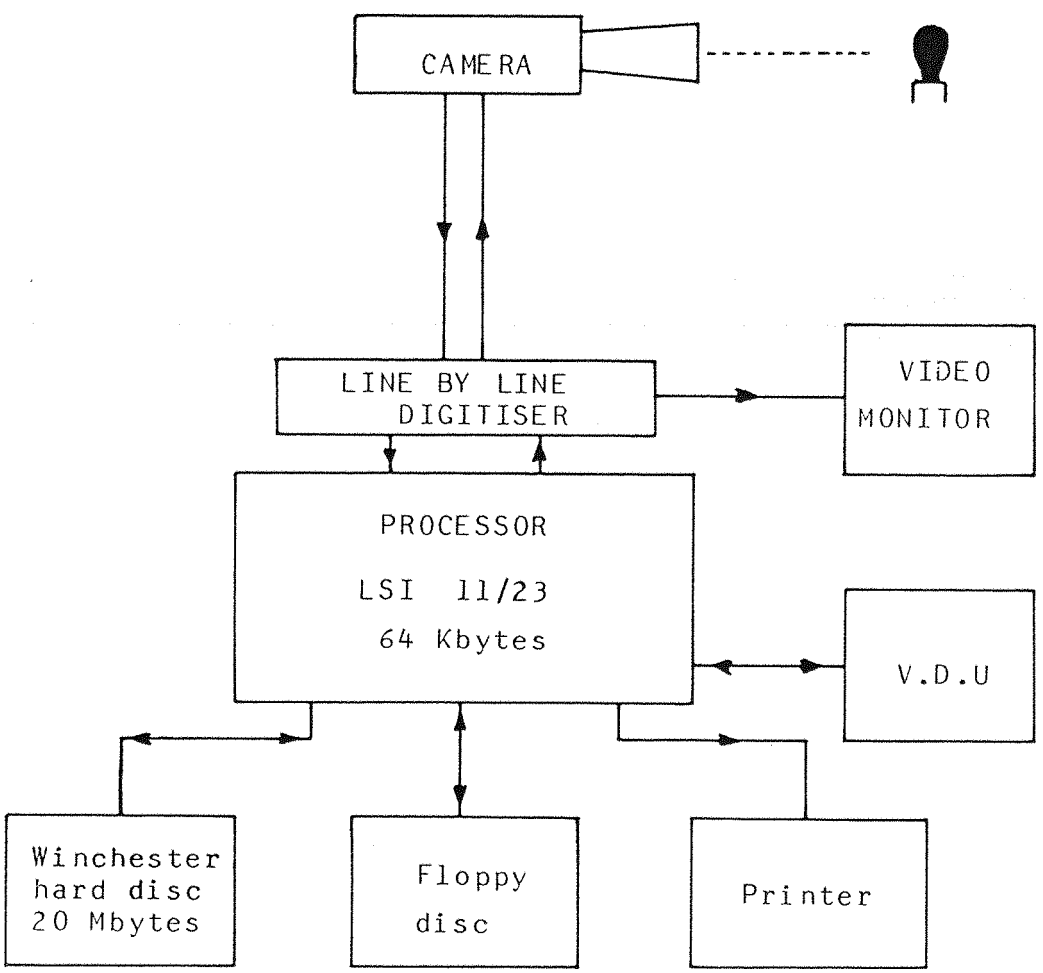

Figure 3.1

3.2. Image recording system

The equipment necessary to produce a video image of a drop consisted essentially of a light source, a thermostated cell, a set of drop forming tips, a macrophotographic lens with extension ring and a video camera. The camera was linked directly to the digitiser placed on the bus of the computer.

3.2.1. Light source

In order to be able to focus the drop image at any ratio of reproduction, a diffuse light source was prefered to the parallel light source used generally in the pendant drop technique. The light was monochromatic (green) to avoid diffraction at the edge of the drop. The focusing was followed on the TV monitor. As shown in figure 3.2, the set up was composed of a 150 Watts halogen lamp (from a cheap slide projector), a monochromatic filter and a tracing paper screen placed as close as possible to the cell. This arrangement provides a uniform background illumination of the drop. All the equipment above mentioned was fixed on to an optical rail and mounted on an anti-vibration table.

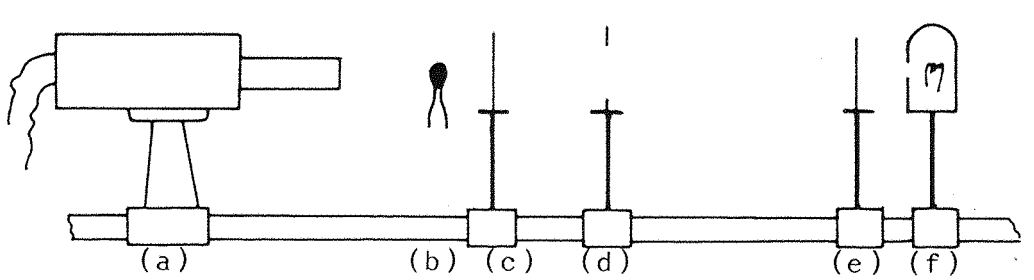

Figure 3.2: Schematic diagram of the optical system used — (a) video camera; (b) drop; (c) tracing paper screen ; (d) iris diaphragm ; (e) green filter ; (e) halogen light source .

3.2.2. Thermostated cell

For working temperatures around 25° C, a water - jacketed glass cell was used. The glass cell was made from a spectrophotometer cell with optical glass windows. Two B 14 joints were added at the bottom and at the top to allow various drop forming tips to be inserted. The water - jacket was made from Perspex and was sealed around the glass cell with silicon rubber. The cell with the water - jacket is shown in figure 3.3.

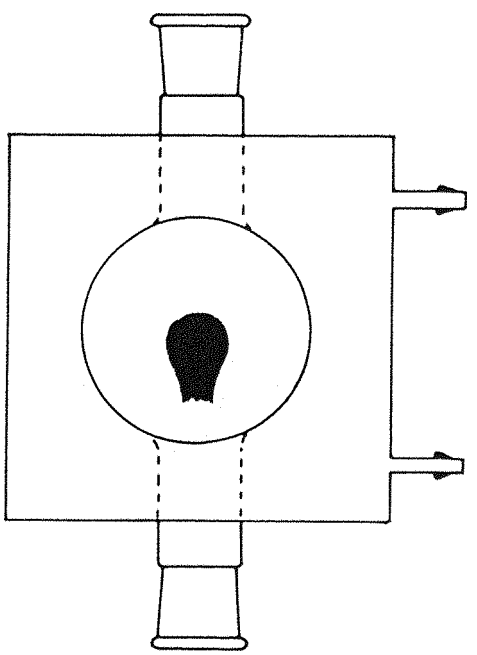

Figure 3.3: Water-jacketed glass cell

The temperature control unit was a circulating thermostat (Gallenkamp, Thermo Stirrer 100,), which has a setting accuracy of ± 0.1° C, but the temperature was constant to a value better than ± 0.05° C.

3.2.3. Drop forming tips

A set of drop forming tips of different sizes was made for this study. For the measurements of interfacial tension between water and nitrobenzene, n-heptane and 1,2-dichloroethane, a range of tips between 3 mm and 7 mm outside diameter was employed.

A tip filling system made up of a reservoir and a 0.2 ml glass syringe was attached to the tips via a B7 joint. The complete set up is shown in figure 3.4.

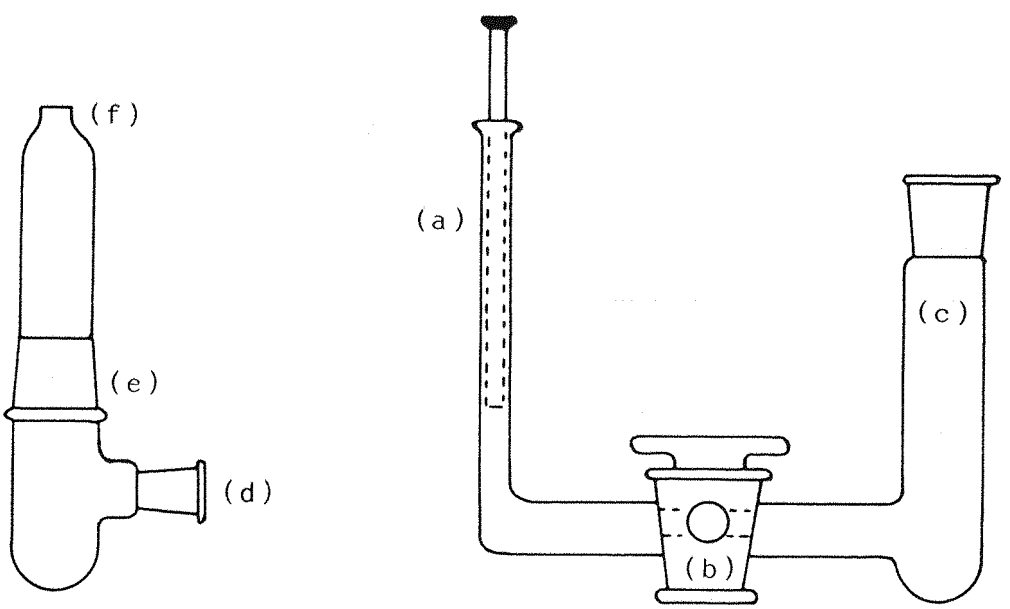

Figure 3.4: Drop forming tip set up.
(a) syringe 0.2 ml ; (b) B7 plug; (c) reservoir; (d) B7 socket; (e) B14 plug; (f) drop forming tip.

3.2.4. Macrophotopraphic lens

The lens used for the interfacial tension studies was a 105 mm Macro Nikon lens fitted with an extension ring Nikon PN-11, which gave continuous focusing with ratios of reproduction between 1 : 2 and 1 : 1 . The choice of a focal length of 105 mm gave a confortable working distance. The relationships for the reproduction ratio of macrophotography are

$$R = \frac{p' - f}{f} = \frac{p'}{p} \qquad (3.1)$$

$$p = \frac{p' \cdot f}{p' - f} \qquad (3.2)$$

where: R = the ratio of reproduction equal to

$$\frac{\text{size of image}}{\text{size of object}} ;$$

f = focal distance of the lens;

p = distance between the object and the lens;

p´ = distance between the image and the lens;

Equation (3.1) and (3.2) were used in the selection of the appropriate lens. In this case the reproduction ratio of 1 : 1 to 2 : 1 was chosen based, on the expected drop size parameters and density differences.

3.2.5. Video camera

The video camera used was a SONY AVC 3250 black and white camera fitted with a 2/3 inch, separate-mesh, vidicon tube. The camera was driven by an external sync system provided by the digitiser, according to C.C.I.R. standard.

3.2.6. Video tape recorder

In order to gain experience in choosing the capillaries, we used a video tape recorder to store the typical drop shape for each capillary. The resolution of the V.T.R. used (SONY VO-2630) was about 300 lines. Therefore, it was not possible to digitise pictures stored on tapes.

3.2.7. Video monitor

The video monitor used was a black and white Hitachi Model VM/910 E/K.

3.3. Digitiser and processor

3.3.1. Introduction to video techniques

3.3.1.1. Introduction to video cameras

Figure 3.5 shows the schematic diagram of a vidicon tube, similar to the one used during this work. It consists of an evacuated glass tube containing an electron gun at one end and the target at the other. The target is a transparent conducting signal plate coated on the scanned face with photo-conductive materials such as antimony trisulphide. A wall anode extends for most of the length of the tube and is connected to a mesh situated about 2 - 3 mm from the target. Line and field deflector coils are grouped around the tube and are surrounded by a focusing coil carrying d.c. which produces an axial magnetic field. More details on camera technology are available in reference 4.

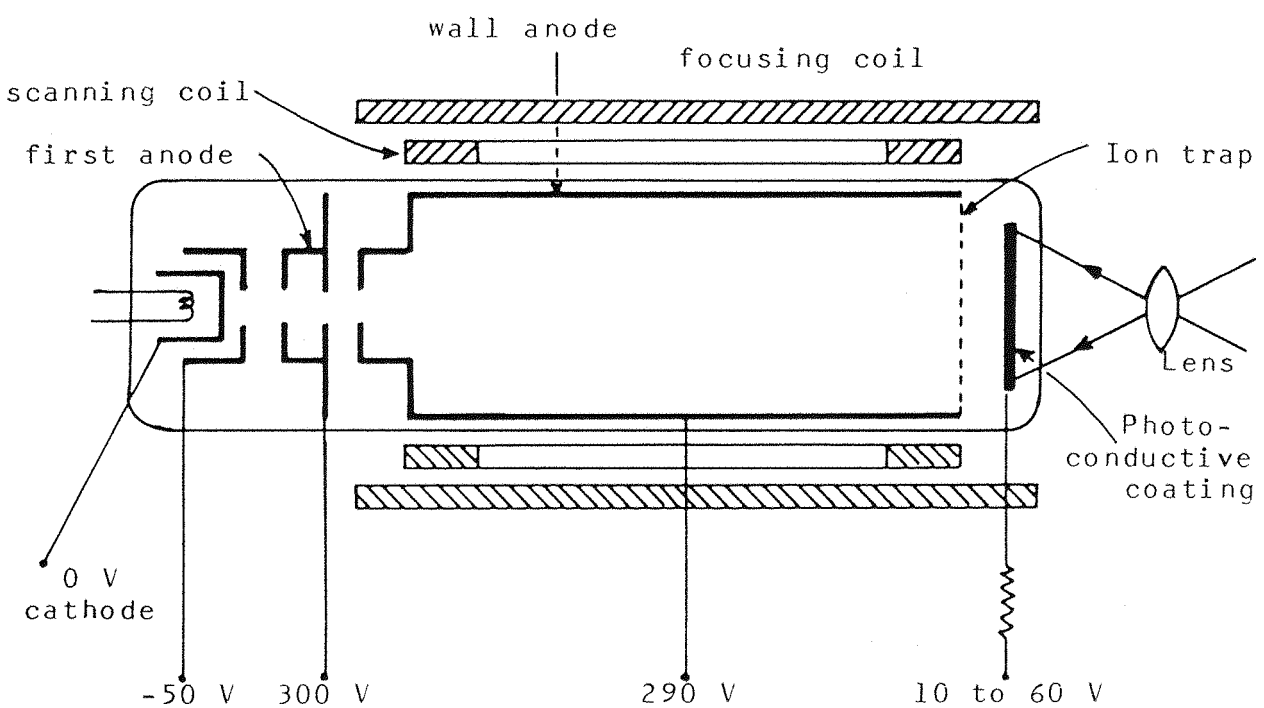

Figure 3.5: Schematic diagram of a vidicon tube

3.3.1.2. Video signal

During a video frame, the video signal coming from the camera is composed of a picture signal and a sync. signal. The picture signal is a mixture of a.c. and d.c. voltage, the d.c. voltage being a function of the total illumination and the a.c. voltage being a function of the grey intensity ranging from the "white level" (maximum a.c. voltage) to the "black level" (zero a.c. voltage) . The d.c. component is compensated at every point of the chain — camera, monitor, video recorder. The sync. signal determines the beginning of a video line. It is composed of rectangular pulses. The picture and sync. signals are combined to produce a single composite signal as shown in figure 3.6.

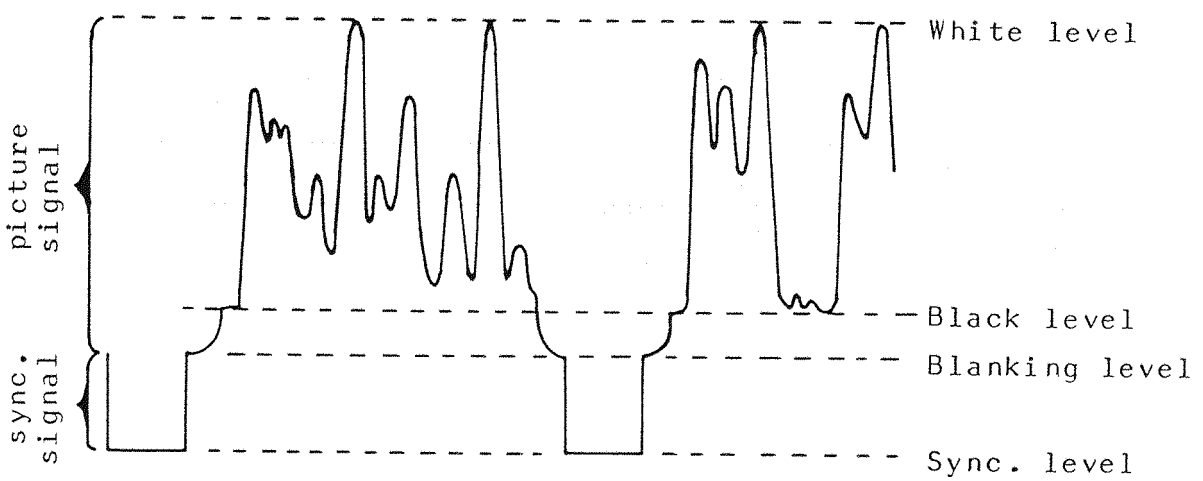

Figure 3.6: Video signal obtained by combining a picture signal with a sync. signal

3.3.1.3. Video frame

In the C.C.I.R. standard used in the United Kingdom, a video frame is composed of 625 lines each having a duration of 64 μsec. The number of video frames per second is 25. The 625 lines are separated in two fields which sequentially form the frame. For convenience, they are called the "odd field" and the "even field". The "odd field"

is composed of the lines 1,3,5,.... and the "even" field of the lines 2,4,6,.... . A schematic diagram of this twin interlacing of a video frame is shown in figure 3.7.

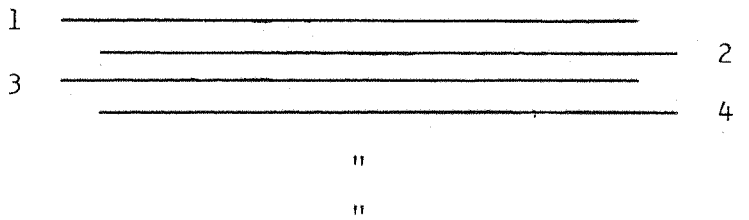

Figure 3.7

3.3.2. Introduction to video image digitisation

3.3.2.1. Video image digitiser

The development of video image digitisation and video image processing has been very fast in the last twenty years. One of the most spectacular applications of this technology is the retransmission of digitised images from planets (Mars, Venus, ...) by satellites.

Nowadays, the main market of image digitisation and image processing is the pattern recognition of items at the end of a production line. The principle of video image digitisation is to divide a video picture into n x n square elements, called pixels (PIC - ture EL - ement). Each pixel can have different levels of grey. Usually, the value of n for commercial digitisers varies from 64 to 256 but can reach 1024 if used with sophisticated cameras. An example of digitised image is shown in Annexe I.

3.3.2.2. Drop image processing with a standard digitiser

As described in Annexe 1, a first attempt of measuring interfacial tension from a video drop image was made with a standard digitiser. The equipment used was SUSIE II[7] (Southampton University System for Image

Evaluation) which is an interactive image processor system. This can acquire, store and process a 128 x 128 video digitised image. Using this system, the processing steps were:

a) Contrast enhancement to make the darkest point in the picture black and the brightest point white; this made the later thresholding stage less sensitive.

b) A histogram plot of ℓn (frequency of occurrence of grey level) vs grey level; this aided the classification of the information into black for the drop and into white for the background.

c) A global threshold of the picture using the grey level value corresponding to the trough in the histogram.

d) Interactive removal of the bright centre of the drop caused by lens effect.

e) Edge detection and final production of a file containing the edge coordinates.

While this approach was experimentally shown to be correct, the video processing was relatively slow (about 3 minutes). For this reason, it was decided to develop, in collaboration with the Department of Electronics at this University, the design and the fabrication of a new digitiser especially adapted to the digitisation of video drop image. The electronic design and the construction was developed by Dr. B.D.V. Smith.

3.3.3. Line by line digitiser

3.3.3.1. Design

The purpose of the construction of a new digitiser was to increase the resolution (128 x 128 pixels) and also to improve the time of data acquisition. The problem was then not to build a bigger and faster

digitiser, but a piece of hardware especially dedicated to the identification of the edge of a video drop image. The idea was then to detect the coordinates of the edge for each of the video lines. If we consider the aspect of a video line (figure 3.9) from a video drop image (schematic representation in figure 3.8), we see that it is possible to detect the edge of the drop image at the step variation in light intensity.

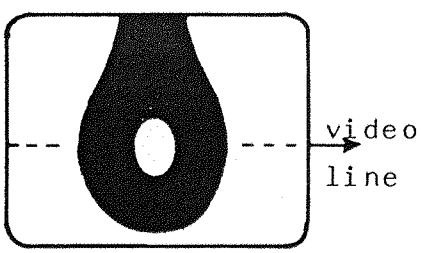

Figure 3.9:
Video image of a pendant drop

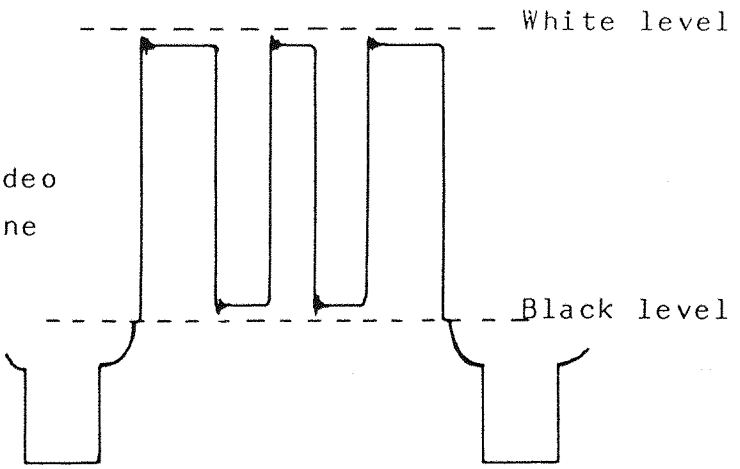

Figure 3.8: Schematic representation of a video line from a video image of a drop

From these figures we see that the detection of the edge can be performed by measuring the time between the sync.-pulse and the first white to black transition and also between the sync.- pulse and the last black to white transition. The central bright area, due to the lens effect, was by this way eliminated.

3.3.3.2. Characteristics

In order to achieve the extraction of the edge of an opaque drop line by line, it was decided to use a real time run code encoding of the binary transitions. This simple technique consists of a counter which is reset synchronously

with the video line sync. pulse and locked with a high speed pixel clock. The output from the counter is then "sampled" at the described edge instants and the count, together with the line number, provides the edge coordinates. The pixel clock must be phase-locked to the video sync. pulses and this is greatly simplified if the pixel clock is divided down to provide the horizontal and vertical sync. pulses and if the camera is supplied with external synchronisation. Use was made of an integrated sync. generator chip operating with a clock of 2.5625 MHz. This clock was in turn provided from the crystal derived pixel clock running at eight times this frequency, i.e. 20.5 MHz. This gave a horizontal resolution of 1 in 1066, and allowing 25 lines per frame for vertical flyback. The overall resolution obtained using a 625 line CCTU camera was of 1066 x 575.

The system had preset controls for hysterisis and threshold level (cf.fig. 3.16). In addition, the edge detected was mixed with the analog video signal to provide a highlight around the drop to enable the user to see the effect of adjustments. A third control was provided to enable the user to move a highlight pair of adjacent horizontal lines up and down the screen at will to terminate the acquisition of data.

The data is transferred at the end of each television line into the computer under direct memory access (DMA). The high speed of this operation means that it is possible to transfer two pairs of coordinates (X_L, Y) and (X_T, Y) into memory during the spot flyback period. Data, therefore, is transferred as it is acquired and double buffering is not necessary. The DMA burst is enabled at the beginning of the video frame under software control, a burst taking place at the end of each line, if there is data to transfer. The beginning of the next frame is then sought through a software loop and DMA disabled when the next field is detected. The central bright area was eliminated during data transfers by choosing only the first white to black transition and the last black to white. This was implemented in hardware using

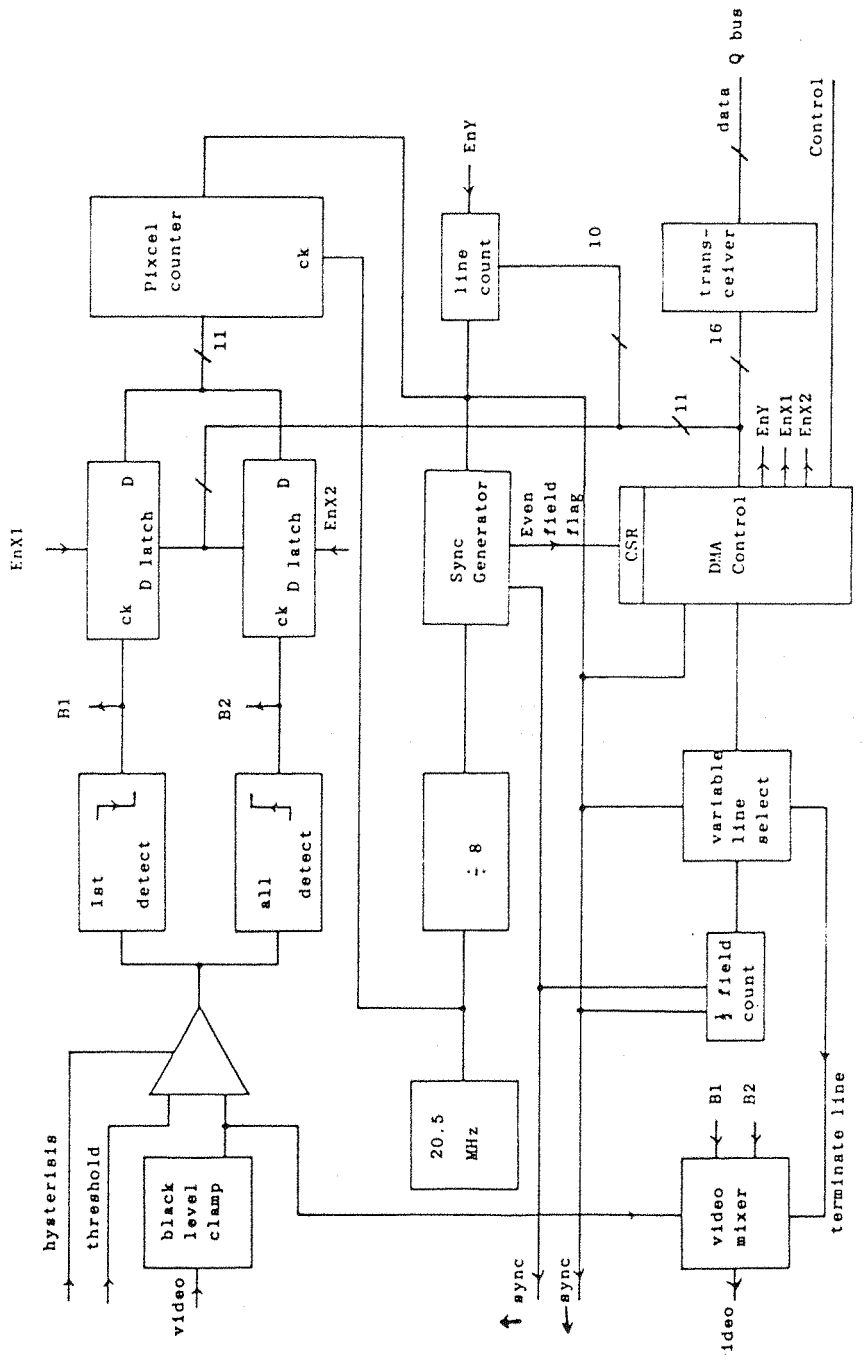

Figure 3.10: Schematic diagram of the line by line digitiser

the horizontal sync. pulse to reset the detection logic. A simplified schematic diagram of the digitiser is shown in figure 3.10.

The hardware was built using a mixture of Schottky and low-power Schottky TTL circuits, using wire-wrap technology for the interconnections.

3.3.4. Processor

The processor used during this work was a Digital PDP 11-23. As described in paragraph § 3.3.3., the digitiser board was placed in the Q-bus of the computer between the processor card and the memory cards. The computer was used with the following peripherals:

a) 20 Mbytes Winchester hard disc;

b) SS-DD floppy disc;

c) Printer (Digital);

d) V.D.U. (Televideo).

3.3.5. Data acquisition

The programs used for data acquisition were written in D.E.C. Macro-11 language by B.D.V. Smith and were supplied as part of the digitiser package.

3.3.5.1. Direct video frame acquisition in memory

This first program written was used to transfer up to 7 consecutive video frames into memory. The limitation to seven frames is due to the fact that the computer used only had a memory capacity of 64 Kbytes. Each frame stored represents a memory array of 4.6 Kbytes. The data can then be directly processed or transferred to the Winchester hard disc.

3.3.5.2. Video frame acquisition on Winchester hard disc

It was observed that the time of transfer from the memory of the processor to the Winchester hard disc was less than 80 ms, which is the time equivalent to two video frames. Therefore, it was possible to make a program where up to 400 frames could be recorded on to the Winchester hard disc. The user was given the possibility of choosing the time interval between two consecutive acquisitions. The minimum time is obviously restricted to the 80 ms necessary for the transfer. A schematic representation of data acquisition on disc is shown in figure 3.11.

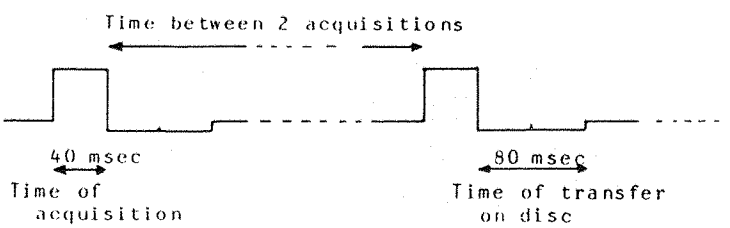

Figure 3.11

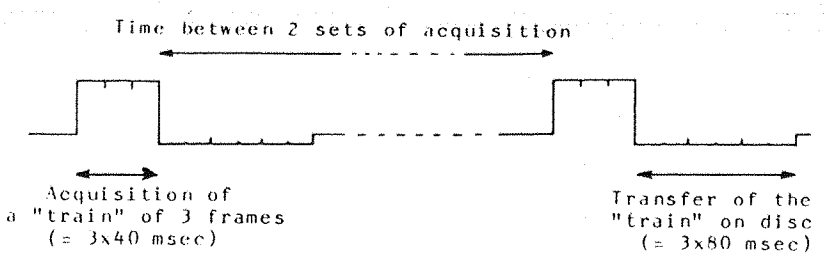

Figure 3.12

This program was used for kinetic studies of adsorption.

At the end of this work a new program was developed in order to acquire a "train" of data so as to allow an averaging at any given time. A schematic representation of this type of acquisition is given in figure 3.12. The "train" size can reach 7 frames. The minimal time necessary to transfer the "train" on the hard disc is in this case twice as long as the "train" duration.

3.4. Calibration

The video camera and the line by line digitiser give an object image composed of 575 lines each having a resolution of 1066 pixels. The dimensions of the image are then given by the digitiser as a number of lines for the vertical axis and as a number of pixels for the horizontal axis, assuming that the camera is used in a horizontal position. A calibration of this difference of units is necessary. This difference is independent of the lens used, but is a constant of the camera and the digitiser. Paragraph § 3.4.1. describes the method used to correlate these units.

The macro lens used had the advantage of a continuous focusing facility for different ratios of reproduction between 2 : 1 and 1 : 1 . The ratio of reproduction was chosen so as to make the image of the drop as large as possible and thus optimize the number of data points. Therefore, for each ratio it was necessary to calibrate the horizontal axis given in pixels into metric units. Paragraph § 3.4.2. describes the method used for this calibration.

3.4.1. Calibration of the vertical axis in pixel units

The ratio of dimensions of a video image is 3 : 4. Since the digitiser transforms the video image into a set of coordinates composed of 575 lines by 1066 pixels, it would be theoretically possible to calculate the relationship between line units and pixel units. However, as seen in paragraph § 3.3.1.3., a video frame is composed of two fields. At the end of each field, a field-sync. signal is introduced and this signal is contained within a period of blanking level called the "field blanking period". In the same way, at the end of each video line, a line-sync. signal is introduced and this signal is also contained within a period of blanking level called the "line blanking level".

Figure 3.13 shows the difference between the complete video frame and the observed picture.

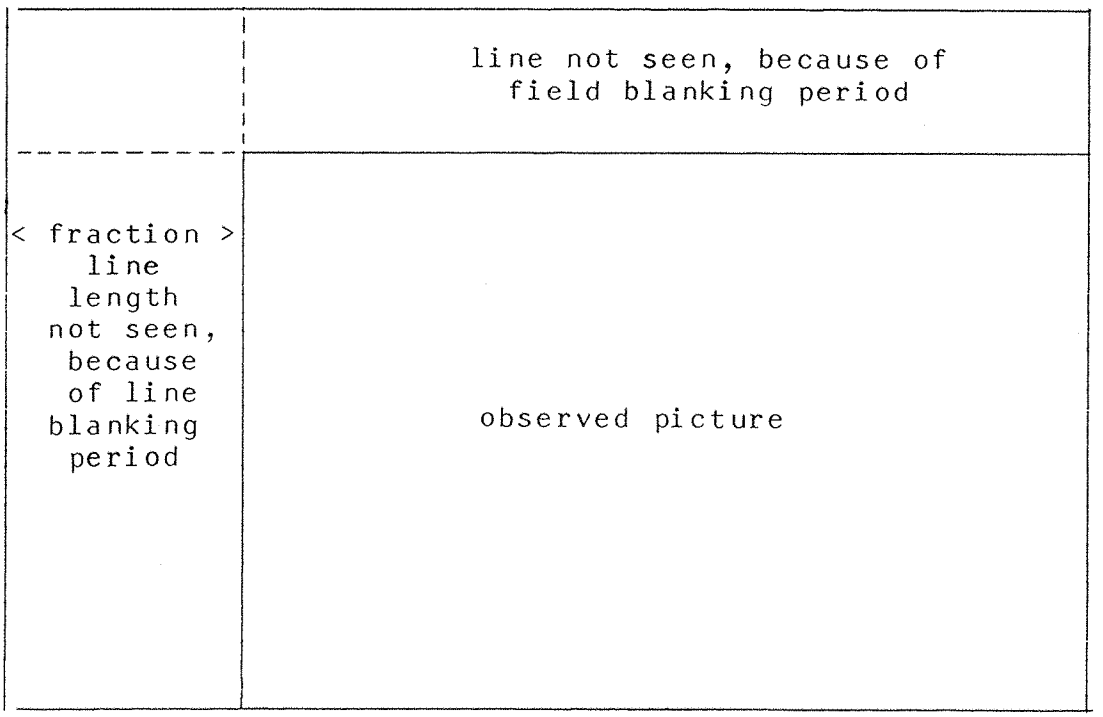

Figure 3.13: Relationship between electrical and observed aspect ratios;

Therefore, a direct calculation is not straightforward and a calibration procedure was preferred. One of the ways to do such a calibration, is to digitise images of patterns of known dimensions, such as squares, rectangles, etc. ... The calibration of the camera, the lens and the digitiser was done by digitising a square pattern. The coordinates of the digitised squares were printed and the ratio line unit : pixel unit was calculated. An extract of the listing, where only 1 line in 20 is shown, is given in Table 3.1 . The alignment of the base of the square with the horizontal video line was carried out using the display of the termination line of the digitiser. However, perfect alignment was never achieved as is shown in the last column of Table 3.1 .

The values for the calibration of the camera and the digitiser were

$$347 \pm 1 \text{ lines} = 511.5 \pm 1.5 \text{ pixels} ,$$

which allow the calculation of the parameter ECHELL, defined in § 2.2.5. :

ECHELL = number of lines per pixel = 0.6784 ± 0.5 % .

Y	X_L	X_T	ΔX	$\frac{X_L + X_T}{2}$
120	411	925	514	668
121	411	925	514	668
"	"	"	"	"
140	412	925	513	668
160	412	925	513	668
180	412	924	512	668
200	412	924	512	668
220	412	923	511	667
240	412	923	511	667
260	411	922	511	666
280	412	922	510	667
300	411	921	510	666
320	411	922	511	666
340	411	921	510	666
360	410	921	511	665
380	409	920	511	664
400	409	920	511	664
420	408	920	512	664
440	407	919	512	663
460	407	920	513	663
"	"	"	"	"
465	407	919	512	663
466	412	920	508	666
467	898	919	21	908

Table 3.1: Extract of a calibration listing of a square pattern

(Y is given in line units and X_L, X_T and ΔX in pixel units.)

3.4.2. Calibration of the horizontal axis

During this study a wide range of drop shapes and dimensions were used. The diameter of the drop varied from 1 mm to 5 mm. The macro lens used with its extension ring had continuous focusing from ratios of reproduction of 2 : 1 (image size equal to half the object size) to 1 : 1 (image size equal to the object size). The ratio was chosen so that the drop image was as big as possible. When the ratio was determined, the focusing of the drop, or of the calibration pattern was carried out by moving the object along the optical rail.

The calibration pattern employed was a stainless steel rod machined with great accuracy. A set of ten rods having dimensions ranging from 2 mm to 12 mm was used. The digitised image of the calibration pattern is a set of coordinates X_L and X_T from which the distance

$$\Delta X = X_T - X_L$$

is calculated for each video line. An average is calculated over the 300 central lines for which the linearity of the camera is best. The calibration was carried out with as many rods as possible; usually three rods were used.

An example of calibration values is given in Table 3.2, where ΔX, X_L and X_T are average values over 300 lines and the values in the first column represent the diameter of the rod used. The table shows that the standard deviation in the reading of X_L, X_T and ΔX is less than 2 pixels. This confirmes the estimation made in paragraph § 2.3.4.

This difference of 0.2 % in the measurement of ΔX has two origins. The first one is due to the camera itself, which gives a non-linear response. This results in an image deformation, which is illustrated in figure 3.14. (The black and white camera used during the development of this project was a standard model, since highly accurate cameras are extremely expensive.)

n mm	ΔX / n pixel·mm^{-1}	$\delta\Delta X$ pixel·mm^{-1}	X_L pixel	δX_L pixel	X_T pixel	δX_T pixel
5	98.824	0.240	398.604	1.108	892.722	2.673
5	98.854	0.240	398.614	1.078	892.886	1.557
5	98.855	0.242	398.678	1.094	892.952	1.254
		1 mm = 98.844 ± 0.00015 %				
6	100.042	0.191	377.778	1.355	978.032	1.445
6	100.069	0.168	377.734	1.442	978.148	1.493
6	100.075	0.137	377.728	1.437	978.180	1.557
		1 mm = 100.062 ± 0.00014 %				
7	99.742	0.263	311.348	1.525	1009.542	1.145
7	99.749	0.265	311.208	1.451	1009.454	1.201
7	99.752	0.282	311.142	1.445	1009.408	1.228
		1 mm = 99.748 ± 0.00005 %				
		SCALE = 99.68 ± 0.48 %				

Table 3.2: Results of calibration of the horizontal axis

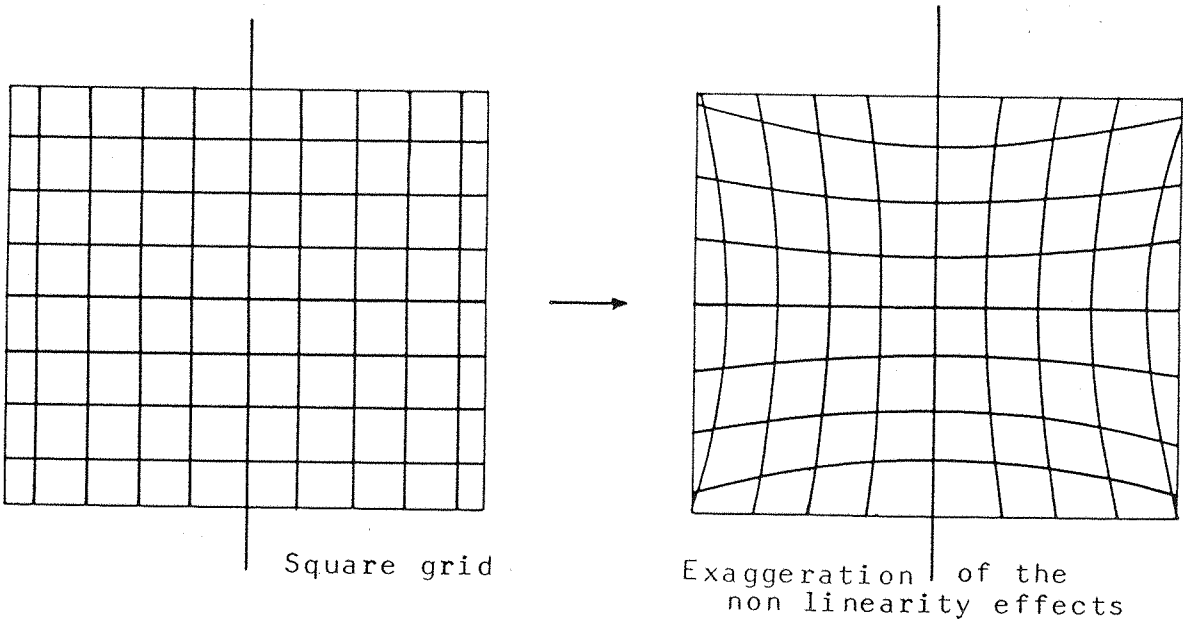

Figure 3.14: Schematic representation of the non linearity of a video camera from the image of a grid

The second source of error is due to the jitter of the detection of the edge of the drop, i.e. the jitter in the measurement of the time between the sync. pulse and the jump in light intensity. The video signal response to an image composed of a black to white transition (cf. figure 3.15) is shown in figure 3.16 with the corresponding clock timing. The slope of the video signal at the jump depends mainly on the quality of the focusing of the calibration rod. If the focus is sharp enough, the slope is theoritically infinite and therefore the incertainty in the detection becomes negligible. This is confirmed by the reproduciblity to better than 0.0001%, obtained during the calibration of a given rod, as shown in Table 3.2.

We may thus conclude that the origin of the error of 0.2 % in the measurement of ΔX is due to the non-linearity of the camera used.

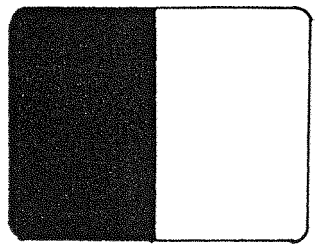

Figure 3.15

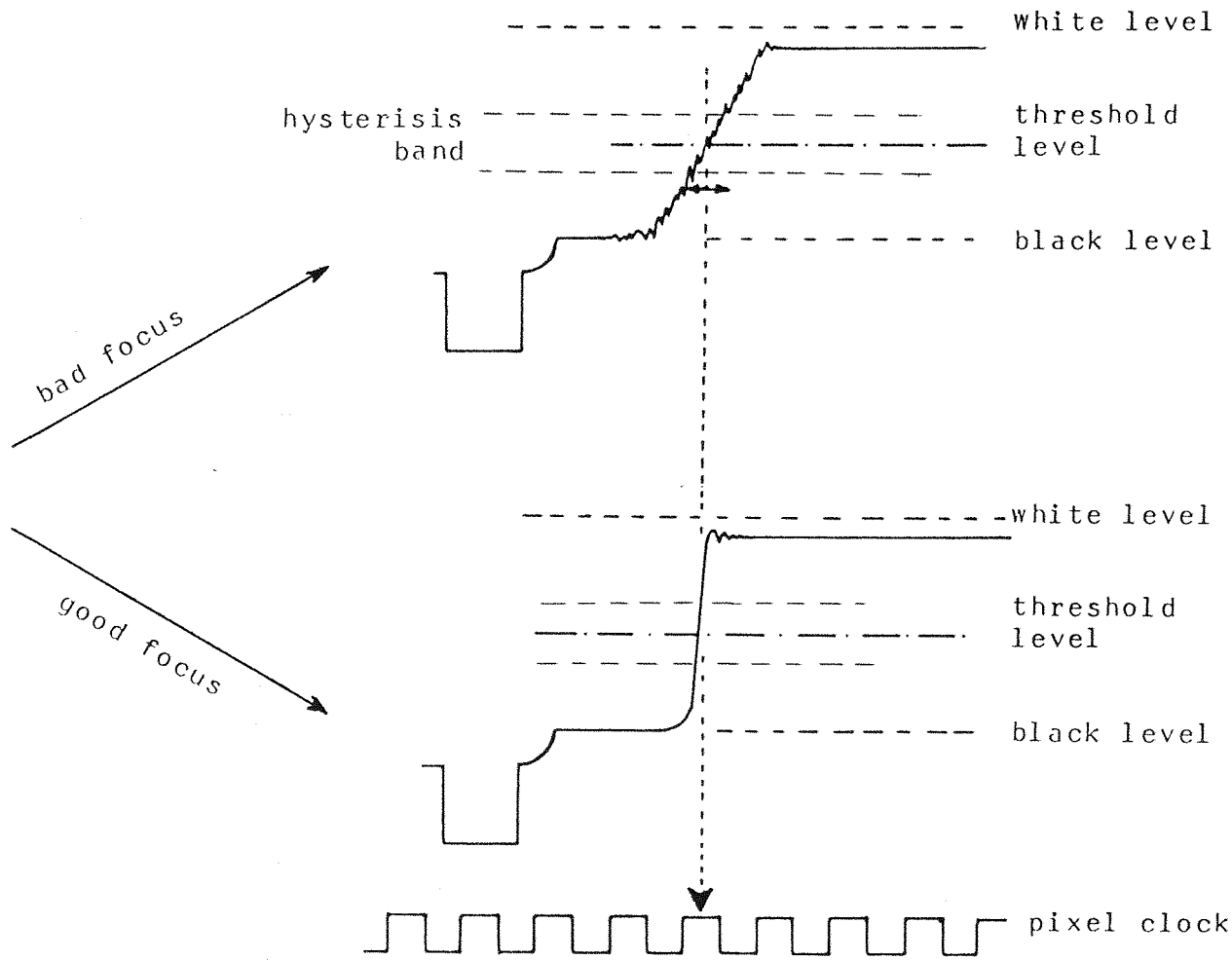

Figure 3.16

PART II

CHAPTER 4

SURFACE CONCENTRATION OF WATER AT THE ITIES

4.1. Introduction

The interfacial properties of immiscible electrolyte solutions have recently been the subject of a great deal of interest[47]. These interfaces can be polarised and little charge transfer can be observed in a potential range of 0.2 to 0.3 Volts when appropriate electrolytes are chosen for each phase[37,61].

However, the potential distribution across these interfaces appears to differ considerably from that occuring in the metal – solution case. Gavach et al[23] proposed an interfacial model consisting of two inner or compact layers separating two diffuse double layers at each phase.

For the mercury – solution interface, it has been argued that the existence of a compact layer results in an excluded ion free layer at the interface. Furthermore, thermodynamic evidence indicates the presence of an ion excluded region at the air – solution surface, due to the solvation of the ions [56].

Recent results by Samec et al.[62] have shown that the rate constant for ion transfer is independent of potential if diffuse layer effects are taken into account. These results throw some doubt on the validity of a separation of the interfacial region into two compact layers, where ions are excluded, and into two diffuse layers, one present in each phase.

The purpose of the present work was to determine the existence and thickness of any ion free layer at an Interface between Two Immiscible Electrolyte Solutions, and thus to derive interfacial structural informations.

4.2. Theory

4.2.1. Adsorption at liquid - liquid interfaces

In the case of a pure liquid-liquid interface, the differential density of the interfacial free energy, defined by equation (4.1)

$$\gamma = \left(\frac{\partial F}{\partial \Omega^{\sigma}} \right)_{T,V,N} , \qquad (4.1)$$

can be identified, due to the isotropy of the interface, to the interfacial tension.

The interfacial tension can be described as a contractile force of γ mN/m acting parallel to the interface. For pure liquids, the spontaneous contraction of a liquid interface is a simple consequence of the tendency of free surface energy to diminish. But in a solution of many components, with different fields of attractive forces round the molecules, there is another mechanism by which the free energy can diminish. Immediatly after a new interface has been formed in a solution, the molecules of that component, which has the smaller field of attractive forces, tend to concentrate at the interface. This interface concentration, called adsorption, decreases the boundary tension.

Equilibrium is reached when the rate of adsorption is equal to the rate of desorption away from the interface. The relation between the quantity adsorbed and the change of surface tension was first given by Willard Gibbs[24] in 1878.

4.2.1.1. Gibbs equation

In order to calculate the Gibbs equation, we should define first the interface as a region between two phases (i.e. Organic/Aqueous), of which the volume and thickness

are not known.

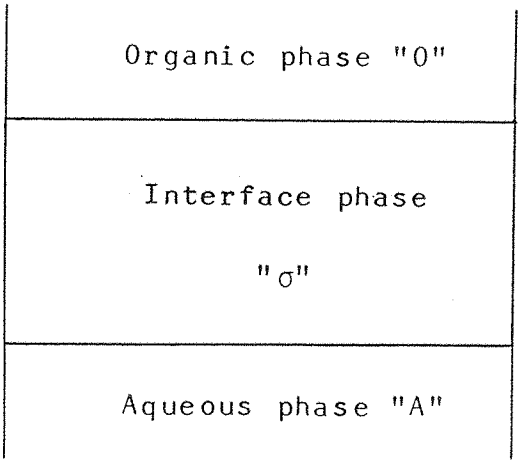

All changes in properties from 0 to A take place through the interface. We can also define the composition of the interface as:

$$\Gamma_{j0} = \frac{N_{j0}^{\sigma}}{\Omega^{\sigma}} = \frac{N_{j0} - n_{j0}^{0} V^{0}}{\Omega^{\sigma}} \qquad (4.2)$$

with: Ω^{σ} = area of the interface;

N_{j0}^{σ} = total number of particles j0 at the interface;

N_{j0} = total number of particles j0 in the system;

n_{j0}^{0} = concentration of j0 in the organic phase.

In the same way, we have:

$$\Gamma_{jA} = \frac{N_{jA}^{\sigma}}{\Omega^{\sigma}} = \frac{N_{jA} - n_{jA}^{A} V^{A}}{\Omega^{\sigma}} \quad .$$

We can also define the Helmholtz free energy of the interface by:

$$F^{\sigma} = F - F^{A} - F^{0} = U^{\sigma} - TS^{\sigma} \quad . \qquad (4.3)$$

The complete differential of F^{σ} is

$$dF^{\sigma} = dU^{\sigma} - TdS^{\sigma} - S^{\sigma}dT \qquad (4.4)$$

with

$$dU^{\sigma} = TdS^{\sigma} - PdV^{\sigma} + \gamma d\Omega^{\sigma} + \sum_{jA} \tilde{\mu}_{jA} \, dN_{A}^{\sigma} + \sum_{j0} \tilde{\mu}_{j0} \, dN_{0}^{\sigma} \qquad (4.5)$$

Equation (4.4) can also be written as:

$$dF^{\sigma} = - PdV^{\sigma} - S^{\sigma}dT + \sum_{j}\sum_{A} \tilde{\mu}_{jA}\, dN_{jA}{}^{\sigma} + \sum_{j}\sum_{0} \tilde{\mu}_{j0}\, dN_{j0}{}^{\sigma} + \gamma d\Omega^{\sigma}, \tag{4.6}$$

if we admit that at the equilibrium,

$$\tilde{\mu}_{j}{}^{A} = \tilde{\mu}_{j}{}^{\sigma} = \tilde{\mu}_{j}{}^{0} \quad .$$

On the other hand, F is also a function of state and can thus be written as

$$F = \sum_{i} \left(\frac{\partial F}{\partial X_i} \right)_{X_{j\neq i}} X_i \quad , \tag{4.7}$$

with X_i representing the extensive parameters of the system, which are, in the case of liquid-liquid interfaces,

$$V^{\sigma},\ \Omega^{\sigma},\ N_{jA}{}^{\sigma},\ N_{j0}{}^{\sigma} \quad .$$

Then one can write

$$F^{\sigma} = - PV^{\sigma} + \gamma\Omega^{\sigma} + \sum_{j}\sum_{A} \tilde{\mu}_{jA}\, dN_{jA}{}^{\sigma} + \sum_{j}\sum_{0} \tilde{\mu}_{j0}\, dN_{j0}{}^{\sigma} . \tag{4.8}$$

By complete differentiation of equation (4.8) we have

$$\begin{aligned} dF^{\sigma} = &- PdV^{\sigma} - V^{\sigma}dP + \gamma d\Omega^{\sigma} + d\gamma\Omega^{\sigma} + \sum_{jA} d\tilde{\mu}_{jA}\, N_{jA}{}^{\sigma} + \\ &+ \sum_{j0} d\tilde{\mu}_{j0}\, N_{j0}{}^{\sigma} + \sum_{jA} \tilde{\mu}_{jA}\, dN_{jA}{}^{\sigma} + \sum_{j0} \tilde{\mu}_{j0}\, dN_{j0}{}^{\sigma} \quad . \end{aligned} \tag{4.9}$$

By comparison of equation (4.6) and (4.9), $d\gamma$ may now be written as

$$d\gamma = - \frac{S^{\sigma}}{\Omega^{\sigma}} dT + \frac{V^{\sigma}}{\Omega^{\sigma}} dP - \sum_{jA} \Gamma_{jA}\, d\tilde{\mu}_{jA} - \sum_{j0} \Gamma_{j0}\, d\tilde{\mu}_{j0} \tag{4.10}$$

which is the general form of the Gibbs equation for adsorption.

For all practical purposes $V^{\sigma}dP$ is negligible. At constant temperatures the Gibbs equation is then reduced to

$$d\gamma = - \sum_{jA} \Gamma_{jA} \, d\tilde{\mu}_{jA} - \sum_{j0} \Gamma_{j0} \, d\tilde{\mu}_{j0} \quad . \qquad (4.11)$$

4.2.1.2. Adsorption of electrolytes

The adsorption of electrolytes at liquid-liquid interfaces may be determined by means of the Gibbs equation in much the same way as for non-electrolytes. The procedure is, however, not quite as straightforward. Consider, for example, a system composed of an organic solvent (organic phase) in contact with an aqueous solution of a salt S (aqueous phase). We can write the Gibbs equation (4.11) as

$$- d\gamma = \Gamma_S \, d\tilde{\mu}_S + \Gamma_{H_2O} \, d\mu_{H_2O} + \Gamma_0 \, d\mu_0 \, , \qquad (4.12)$$

if we neglect the presence of H^+ and OH^- . Unless a definite restriction can be placed on the distribution of the components between the two phases, it is difficult to proceed much beyond equation (4.12). Simplification of this equation can be effected if we assume the following restraint:

> the concentration of the salt is negligible in the organic phase.

Therefore, the Gibbs - Duhem equation, applied to the organic phase, is reduced to

$$n_0^{(0)} \, d\mu_o^{(0)} + n_{H_2O}^{(0)} \, d\mu_{H_2O}^{(0)} = 0 \qquad (4.13)$$

The Gibbs - Duhem equation, applied to the aqueous phase, gives

$$n_S^{(A)} \, d\mu_S^{(A)} + n_{H_2O}^{(A)} \, d\mu_{H_2O}^{(A)} + n_0^{(A)} \, d\mu_0^{(A)} = 0 . \qquad (4.14)$$

By substituting the equations (4.13) and (4.14) into equation (4.12), we have

$$\frac{-d\gamma}{RT} = \left[\left(\Gamma_{H_2O} - \frac{n_{H_2O}^{(A)}}{n_S^{(A)}}\Gamma_S\right) - \frac{n_{H_2O}^{(0)}}{n_0^{(0)}}\left(\Gamma_0 - \frac{n_0^{(A)}}{n_S^{(A)}}\Gamma_S\right)\right] d\ell n a_{H_2O} \qquad (4.15)$$

From this equation, it is possible to define the quantity $\Gamma_{H_2O}^{(S)}$ and $\Gamma_0^{(S)}$ respectively:

$$\Gamma_{H_2O}^{(S)} = \Gamma_{H_2O} - \frac{n_{H_2O}^{(A)}}{n_S^{(A)}}\Gamma_S \qquad (4.16)$$

$$\Gamma_0^{(S)} = \Gamma_0^{(S)} - \frac{n_0^{(A)}}{n_S^{(A)}}\Gamma_S \qquad (4.17)$$

$\Gamma_{H_2O}^{(S)}$, represents the surface excess concentration of water with respect to the salt, i.e. the number of moles of water per unit area of interface less the number of moles of water in that part of the aqueous bulk region containing the same number Γ_S of moles of salt.

By analogy, $\Gamma_0^{(S)}$, is the surface excess of organic solvent with respect to the salt. $\Gamma_0^{(S)}$ represents the number of moles of organic solvent per unit area of interface, less the number of moles of organic solvent in that part of the bulk aqueous region which contains Γ_S moles of salt.

By substituting equations (4.16) and (4.17) into equation (4.18), we obtain

$$-\frac{d\gamma}{RT} = \left[\Gamma_{H_2O}^{(S)} - \frac{n_{H_2O}^{(0)}}{n_0^{(0)}}\Gamma_0^{(S)}\right] d\ell n a_{H_2O} \quad . \qquad (4.18)$$

4.2.1.3. Interface between liquids of low mutual miscibility

In the case where the solvents have a low mutual miscibility, equation (4.18) can be reduced to a simpler expression as is demonstrated later.

During the course of this work, three solvents having a very low miscibility with water were used:

a) n-heptane,

b) 1,2-dichlorethane,

c) nitrobenzene.

Table 4.1 gives the different values of:

a) the molar fractions of solvent in water, $n_0^{(A)}$,

b) the molar fraction of water in the organic phase, $n_{H_2O}^{(0)}$,

c) the degree of miscibility, d_m, equal to $n_0^{(A)} + n_{H_2O}^{(0)}$,

d) the ratio $n_0^{(A)}/n_S^{(A)}$ in the case of a bimolar aqueous solution of a salt S.

solvent / molar fraction	n-heptane	1,2-DCE	nitro-benzene
$n_0^{(A)}$	$9\ 10^{-6}$ [9]	$1.6\ 10^{-3}$ [38]	$3\ 10^{-4}$ [9]
$n_{H_2O}^{(0)}$	$8.4\ 10^{-4}$ [9]	$8.8\ 10^{-3}$ [43]	$1.7\ 10^{-2}$ [9]
dm	$8.5\ 10^{-4}$ †	$1.0\ 10^{-2}$ †	$1.7\ 10^{-2}$ †
$\frac{n_0^{(A)}}{n_S^{(A)}}$	$2.5\ 10^{-4}$ †	$4.4\ 10^{-4}$ †	$8.2\ 10^{-2}$ †
$n_S^{(A)}$	$3.6\ 10^{-2}$ †	$3.6\ 10^{-2}$ †	$3.6\ 10^{-2}$ †

Table 4.1 († = calculated value)

Figure 4.1 shows a schematic expected concentration profile of the components present in the interfacial region. From this figure, it is possible to visualize the relative values Γ_0, Γ_S and Γ_{H_2O} .

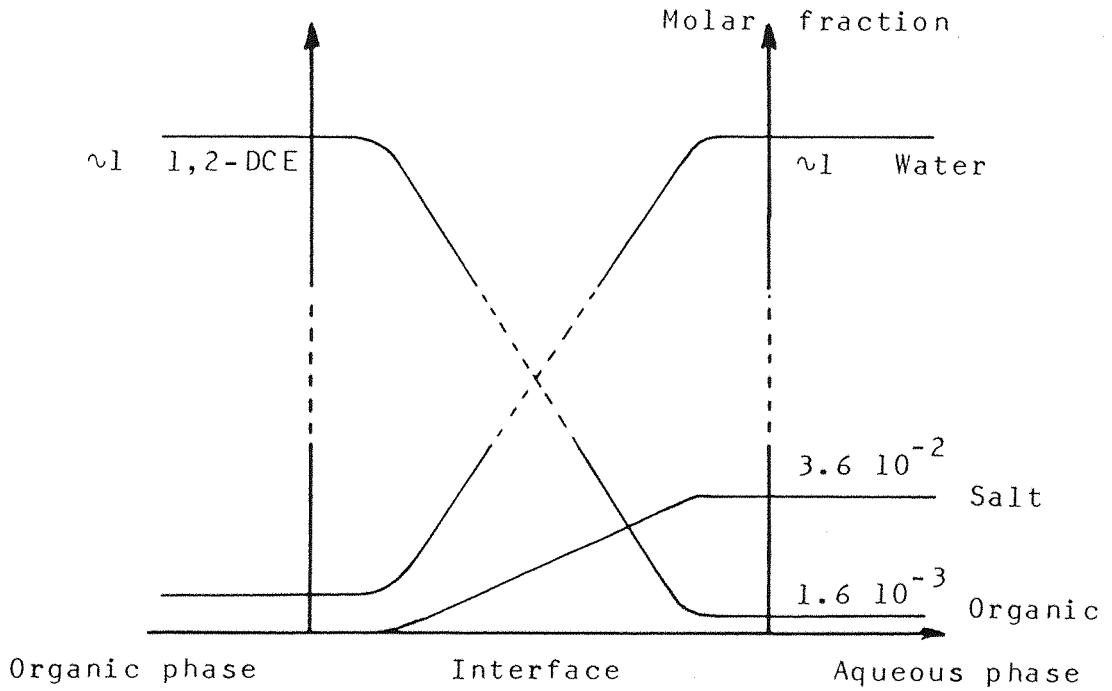

Figure 4.1: Concentration profile of the 1,2-dichloroethane — water interface

Looking at figure 4.1 and using values from Table 4.1 , we can see that the second term of equation 4.17

$$\Gamma_0^{(S)} = \Gamma_0 - \frac{n_0^{(A)}}{n_S^{(A)}} \Gamma_S \qquad (4.17)$$

becomes negligibly small compared to Γ_0 as

$$\Gamma_0 >> \Gamma_S >> \frac{n_0^{(A)}}{n_S^{(A)}} \Gamma_S \ . \qquad (4.19)$$

We can also see from Table 4.1 that in all the different systems studied

$$n_{H_2O}^{(0)} < 2\ \% \quad . \tag{4.20}$$

Therefore, if we further assume that Γ_0 and Γ_{H_2O} are rather similar in magnitude, we see then that by neglecting

$$\frac{n_{H_2O}^{(0)}}{n_0^{(0)}} \Gamma_0^{(S)}$$

with respect to $\Gamma_{H_2O}^{(S)}$, an error of less than 2 % is introduced in the determination of $\Gamma_{H_2O}^{(S)}$. Thus, in this case of the interface between two solvents having low mutual solubilities, equation (4.18) is reduced to

$$-\frac{d\gamma}{RT} = \Gamma_{H_2O}^{(S)}\, d\ell na_{H_2O} \quad . \tag{4.21}$$

4.2.1.4. Analogy with the air-electrolyte solution interface

The Gibbs equation, when applied to the adsorption of electrolytes at the air-water interface, is given by equation (4.22) which is similar to equation (4.21)

$$-\frac{d\gamma}{RT} = \Gamma_{H_2O}^{(S)}\, d\ell na_{H_2O} \quad , \tag{4.22}$$

where $\Gamma_{H_2O}^{(S)}$ is the surface excess concentration of water, as defined by equation (4.16).

The measurement of $\Gamma_{H_2O}^{(S)}$ has been done experimentally for a whole variety of salt solutions. Harkins[34,35] and later Jones and Ray[39-41] observed that the surface tension of many aqueous inorganic electrolyte solutions increased

with increasing concentration of the electrolyte, which thus indicated that the electrolyte as a whole is desorbed from the interface.

The most convenient way to interpret this desorption is in terms of ion-free layers of water at the surface. This model assumes that below the ion-free layer of water at the surface of thickness δ, the electrolyte solution is uniform as shown in figure 4.2.

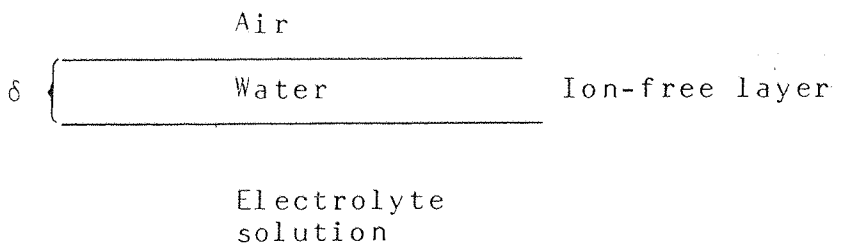

Figure 4.2

This means that the surface excess concentration of water is equal to the quantity of water present in this layer. Figure 4.3 is a diagram showing the concentration profile across the interface; $\Gamma_{H_2O}^{(S)}$ is represented by the shaded area.

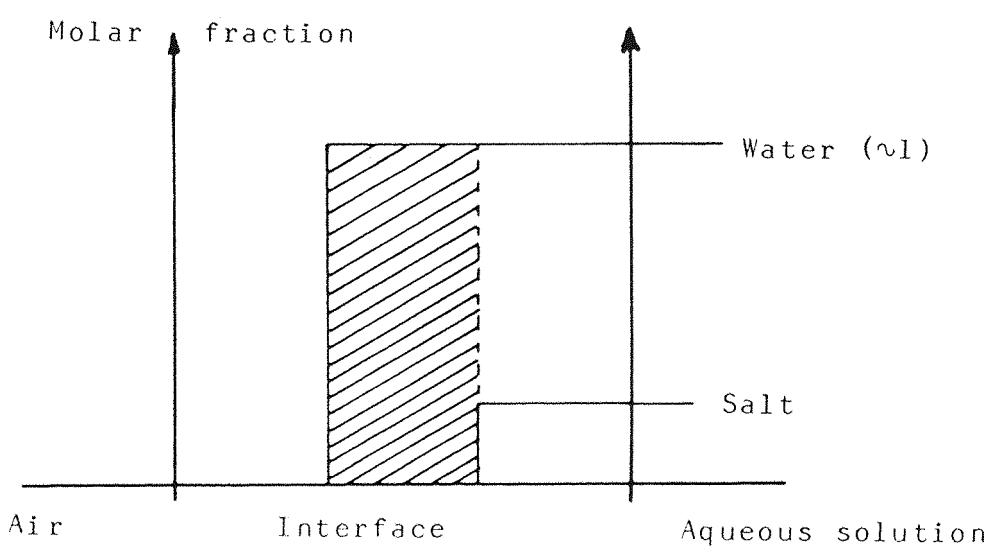

Figure 4.3: Concentration profile at the air – water surface according to the ion-free layer model

The volume per unit area of the ion-free layer of thickness δ is then δ cm^3 per cm^2. If we consider the molecular volume of water to be 18 $cm^3 \cdot mole^{-1}$, it is possible to calculate the number of molecules of water, n, contained in one cm^3, i.e.

$$n = \frac{N}{V} = \frac{6.02 \cdot 10^{23}}{18} = 3.34 \cdot 10^{22} \text{ molecules} \cdot cm^{-3} \quad .$$

Therefore, the number of molecules present in one face of the cube can be approximated to be $n^{2/3}$, where

$$n^{2/3} = 1.04 \cdot 10^{15} \text{ molecules} \cdot cm^{-2} \quad ,$$

which is equivalent to $1.72 \cdot 10^{-9}$ moles per cm^2 .

The surface excess concentration can then be given as a number of monolayers of water, y, by

$$y = \frac{\Gamma_{H_2O}^{(S)}}{1.72 \cdot 10^{-9}} \quad , \qquad (4.23)$$

in which y is not necessarily an integer number.

In 1963, Randles[56] reviewed the different studies on the ion-free layer at the air-water interface and pointed out that the thickness of the water layer was quite independent of the concentration of the electrolyte. This independence was explained by the following general picture. The plane of closest approach of monatomic monovalent ions, such as Li^+, Na^+, K^+ and also F^- and $C\ell^-$, is limited by the hydration shell of the ion, which is usually considered to be one water molecule thick. This explains why the values of $\Gamma_{H_2O}^{(S)}$ measured for these salts are equal to one monolayer.

4.3. Experimental

The technique of measurement of the interfacial tension has been described fully in Part I of this work.

The chemicals used during this work were AnalaR grade reagents. The solvents were washed twice with triply distilled water. The two phases (i.e. organic and aqueous) were first brought to equilibrium by shaking in a separating funnel. They were then separated at room temperature. The electrolyte solution was usually placed in the capillary to act as a drop and the organic solvent as a medium in which to form the drop. The organic solvent was covered by a layer of electrolyte solution to ensure the equilibrium at 25° C, as shown in figure 4.4 .

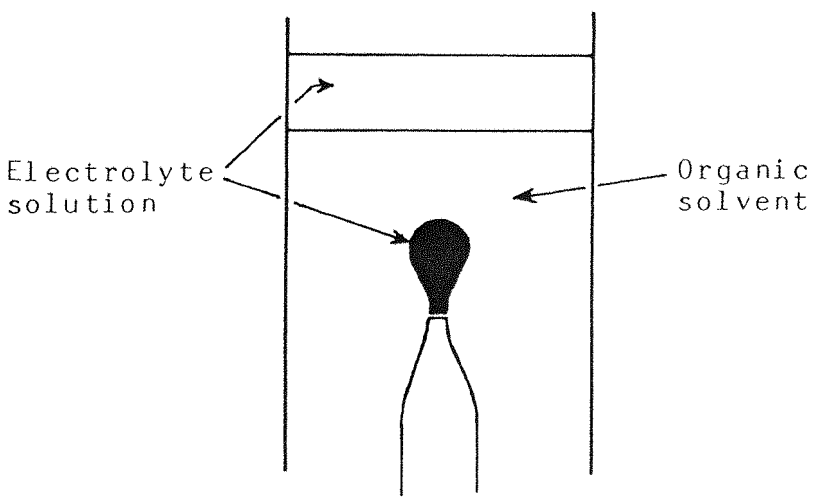

Figure 4.4:

All the results were obtained at 25° C.

4.4. Results

The study of the surface excess concentration of water at the ITIES was carried out using the salts and solvents as shown in Table 4.2 .

	Nitrobenzene	1,2-DCE	n-Heptane
LiCℓ	†	†	†
NaCℓ	†	†	
KCℓ	†	†	†
$MgSO_4$	†		

Table 4.2: Systems studied

The calculation of $\Gamma_{H_2O}^{(S)}$ was achieved by plotting the interfacial tension as a function of $\ell n\ a_{H_2O}$. This value is related to the concentration of the salt by

$$- \ell n\ a_{H_2O} = \frac{18\ \nu\ m\ \phi}{1000} \quad , \qquad (4.24)$$

where ν = the number of ions produced by one electrolyte molecule;

m = the molality of the salt;

ϕ = the molal osmotic coefficient.

It was assumed at the start of the experiment that $\Gamma_{H_2O}^{(S)}$ was constant for a given salt. To find that value, we measured the interfacial tension between an organic solvent and a given electrolyte solution at least for 5 different concentrations. $\Gamma_{H_2O}^{(S)}$ was then calculated by linear regression. These concentrations were selected such that a regular distribution of values of $\ell n\ a_{H_2O}$, as calculated from equation (4.24), were obtained. For each selected concentration, the values of the molality and the density of the solution were read from references[32,38], and the value of the molal osmotic coefficient was taken from reference[57] . All the values used during this work are to be found in Annexe 2.

Figures (4.3), (4.4) and (4.5) show the variation of the interfacial tension as a function of $\ell n\ a_{H_2O}$ for the n-heptane — , 1,2-dichloroethane — and nitrobenzene — water interfaces respectively.

Table (4.2) gives the different values of the surface excess concentration of water at the ITIES, calculated from figures (4.3-5). The values for the surface excess concentration of water at the air — water and the mercury — water interfaces are taken from the literature mentioned in the table.

	LiCℓ	NaCℓ	KCℓ	$MgSO_4$
Φ-NO_2 - water	0.4	0.7	0.4	3.0
1,2-DCE - water	0.4	0.9	0.6	—
heptane - water	0.9	—	1.0	—
Air - water	0.9	1.0	1.0	2.4
Mercury - water	0.8	0.8	—	1.5

Table 4.2: Surface Excess Concentration of water

It was unfortunate that nitrobenzene, like acetophenone, could not be used as a pure solvent as it is photodegradable. The instability of this solvent was observed during this study and explains why the standard deviations of the measurements obtained for the water — nitrobenzene interface were greater than those observed with other organic solvents.

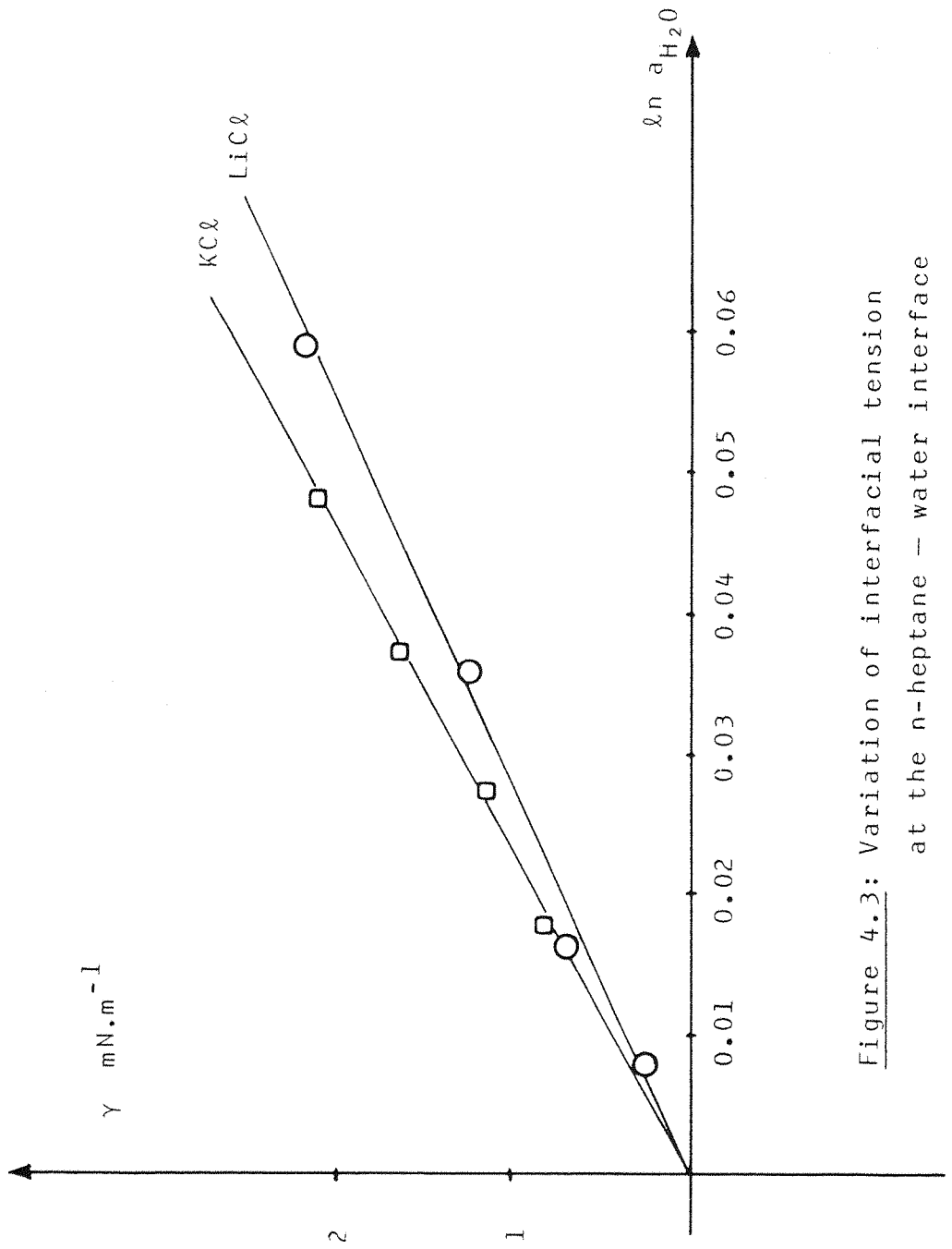

Figure 4.3: Variation of interfacial tension at the n-heptane – water interface

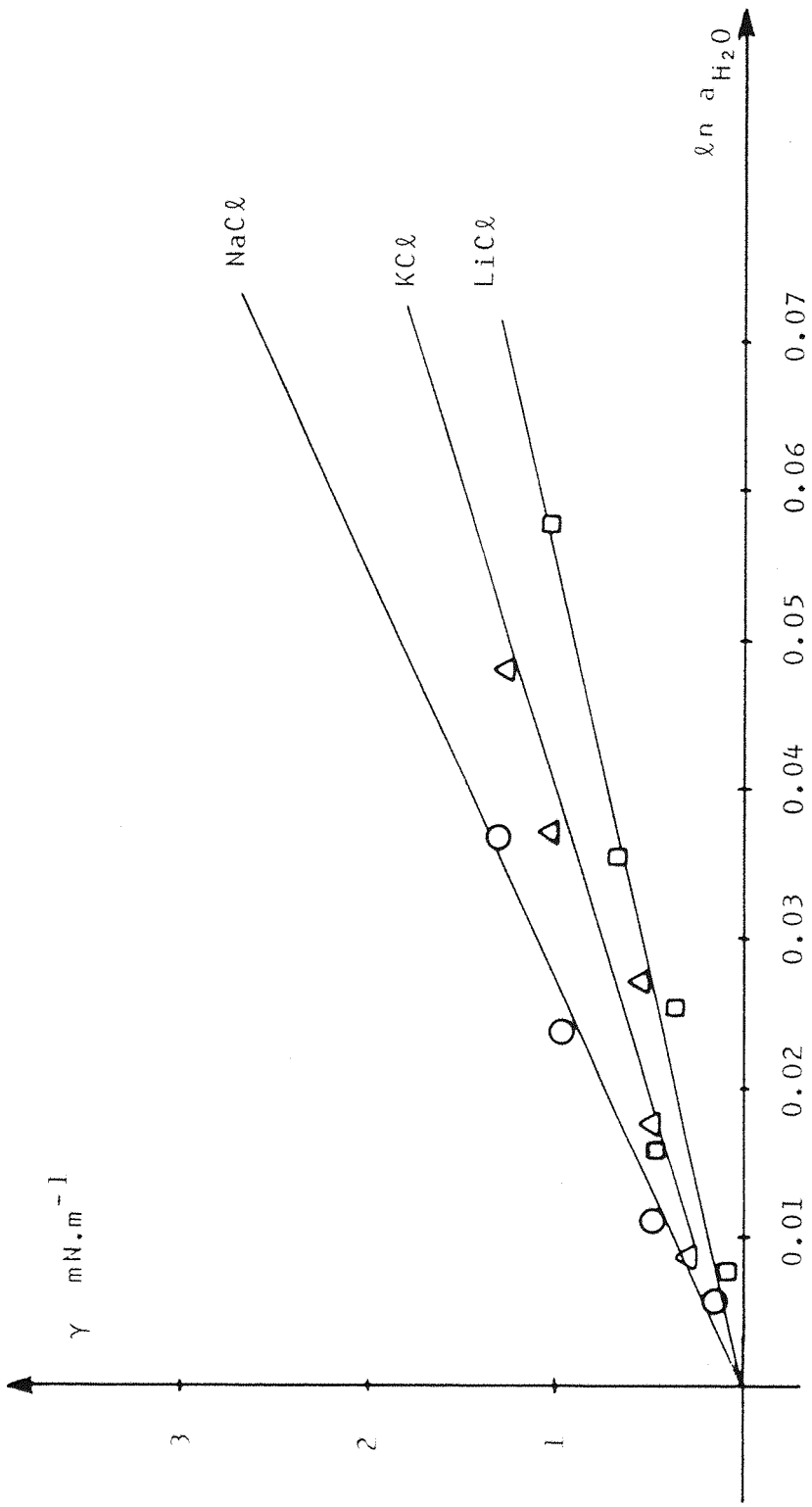

Figure 4.4: Variation of the interfacial tension at the 1,2-dichloroethane – water interface

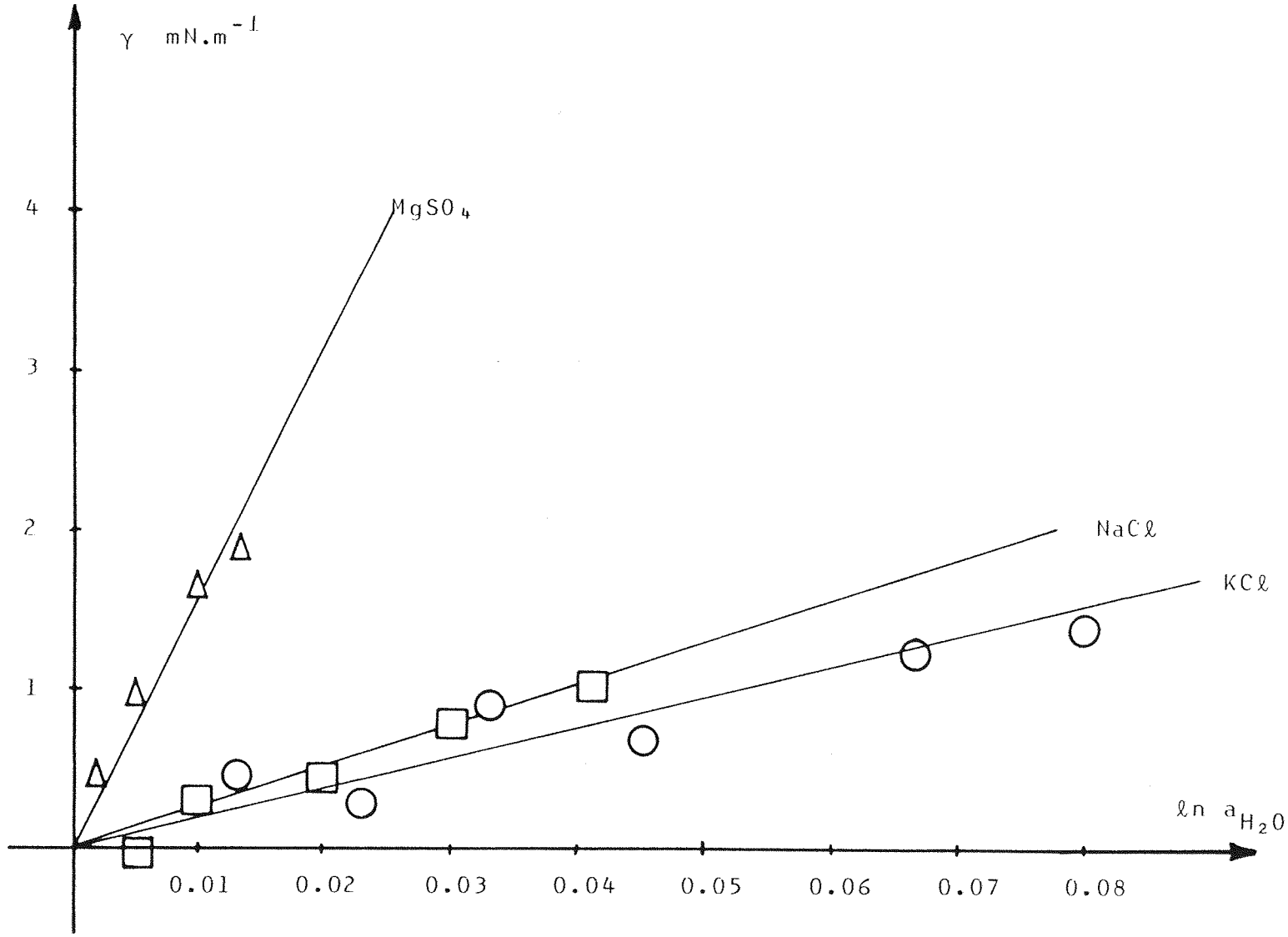

Figure 4.5: Variation of interfacial tension at the nitrobenzene – water interface

4.5. Discussion

4.5.1. Development of the experiment

At the start of this work, we wanted to see whether the surface excess concentrations of water, $\Gamma_{H_2O}^{(S)}$, at the water – nitrobenzene interface for different salts was similar to that observed at the water – air and mercury – water interface. The choice of nitrobenzene was due to the fact that this solvent had been widely used before in electrochemical studies of the ITIES.

The results obtained for this interface showed that for alkali-metal chloride solutions, $\Gamma_{H_2O}^{(S)}$ was smaller than one monolayer. The substantial difference in behaviour between this interface and the water – air surface led us to measure $\Gamma_{H_2O}^{(S)}$ at the interface between a completely non-polar solvent and water. n-Heptane was used here for a set of experiments, and the results obtained were in agreement with those of the air – water surface.

Thus to complete this investigation, we measured $\Gamma_{H_2O}^{(S)}$ for yet another polar organic solvent having this time a lower miscibility with water than nitrobenzene, e.g. 1,2-dichlorethane.

4.5.2. Interpretation of the results

The results presented in Table 4.2 point towards a dependence of the surface excess concentration of water at the ITIES on the polarity of the organic solvent. The good agreement between the results obtained for the non-polar solvent – water interface and those for the air – water surface indicates that the model described by Randles[56] for this surface might also be applicable to an ITIES. We may then postulate here the existence of a plane of closest ionic approach for which the position is determined by the number of hydration layers around the ions.

The interpretation of the results obtained for systems composed of an organic polar solvent and water is much more complex. First of all, nitrobenzene and 1,2-DCE are more soluble in water than n-heptane (cf. Table 4.1) and therefore, it is quite possible that the interface is composed of a mixture of water and organic solvent molecules. If this is so, the ability of an ion to approach or penetrate this liquid mixture layer would be dependent on its size and its degree of hydration.

But the presence of ions in this mixture layer could lead to the possibility of mixed solvations of the ions, especially for the "big" ions like Cs^+, Rb^+ and probably K^+ and Na^+ . Indeed Abraham[1] , in a study of the partition coefficients of ions between water and 1,2-DCE, showed that the alkali-metal and halide ions in 1,2-DCE saturated with water were not hydrated except for Li^+, F^- and $C\ell^-$ ions. Obviously, any model postulating the presence of a mixed solvents layer will be further complicated by the possible formation of ion-pairs at the interface.

One of the interesting points to note from the results given in Table 4.2 is the low value of $\Gamma_{H_2O}^{(S)}$ obtained for the lithium chloride solutions in contact with nitrobenzene and also 1,2-dichloroethane. The Li^+ ion has been described by Frank and Evans[15] as a strong "structure maker" which means that the cation is surrounded by an inner rigidly held layer of water molecules. This layer of strongly orientated dipoles tends to structure the other solvent molecules around it. Therefore, it is most probable that the presence of Li^+ ions near the interface may perturb the structure of that interface by increasing, for example, the miscibility of the two solvents.

The concept of the "structure making" or "structure breaking" capacity of an ion has been recently studied by Abraham *et al.*[2] for non aqueous solvents. He concluded that the alkali-metal cations and the halide anions are all "structure makers" in solvents like 1,2-DCE, whereas they are

"structure breakers" in water, except for Li^+ and Na^+ ions. Therefore, even if the assumption of the presence of a mixture layer at the interface is not valid, it is likely that the presence of ions in the neighbourhood of the organic phase does cause a pertubation of the interface.

4.5.3. Conclusion

From the discussions presented in this chapter, we can deduce that any simple model of the interface is insufficient because of the possible presence of

a) a mixed solvent layer at the interface;

b) the mixed solvation of ions;

c) the formation of ion-pairs;

d) the pertubation of the interface by the "structure making or breaking" effect of the ions.

Thus, in this way, some doubt is cast on the model based on a compact layer composed of orientated water molecules at the ITIES. This model, as the ion-free layer model, implies that the surface excess concentration of water is greater than one monolayer, which is obviously not validated by these experiments. Although it is most likely that the organic solvent involves an orientation of the water dipoles by a hydrophobic effect, it is not necessary that this induced orientation results in the formation of a compact layer.

Furthermore, the presence of ions at the interface is not to be neglected as already, when in the bulk aqueous phase, they create around them a change in the structure of the water molecules. Thus, when they approach the interface it is probable that they will change the structure of that interface. Along this line, it would be very interesting to study the influence of hydrophobic ions such as tetraalkylammonium cations on the surface excess concentration of water.

The picture emerging from the above discussion is in disagreement with the concept of the existance of compact layers at the ITIES. The variations of the surface excess concentration of water with the polarity of the aprotic organic solvent and the ionic size indicates that there is no sharp boundary layer at the ITIES as for example the outer Helmholtz plane at the mercury - solution interface. Indeed, it seems unlikely that, at least for alkali metal chlorides, a charge free dielectric layer of either water or polar organic solvent is present, but the interface must rather be regarded as changing its composition continuously from one medium to the other.

Finally, it ought to be mentioned that these results are in good agreement with the work of Samec et al.[62] who observed that the potential drop across the compact layer remains constant and close to zero regardless of the total potential drop across the interface.

4.6. If it was to be repeated ....

As for most other research students who have reached this stage in their work, it becomes easy to postulate *a fortiori* a much improved experimental technique with which the study could have been carried out.

The measurements of $\Gamma_{H_2O}^{(S)}$ for any given system composed of an electrolyte solution and an organic solvent could have been performed without the *a priori* assumption that this value is constant. By making use of the drop image processing technique, it would have been possible to make a cell containing a known volume of water to which small quantities of concentrated salt solutions could have been added dropwise. Obviously, in this case, the pendant drop would be that of the organic solvent hanging down into the aqueous medium.

Then instead of having a curve $\gamma = f\left[\ \ell n\ a_{H_2O}\ \right]$ composed of 5 to 7 points, for which an error is introduced in focusing the drops each time the concentration is changed, we could have obtained a point by point curve with greater accuracy and in a much shorter time.

This technique would be a sort of "differential" measurement since the calibration of the system would be done initially on the water – organic solvent interface.

PART III

CHAPTER 5

KINETIC MEASUREMENTS OF THE ADSORPTION OF CYTOCHROME C

5.1. Introduction

The purpose of this chapter is to illustrate the capabilities of the line by line digitiser in the study of kinetic effects such as in adsorption.

Indeed, we had already tried to study the adsorption phenomena using the first method of drop image processing which we had developed in 1981 (cf. Annexe I). The technique involved the recording of the life of a pendant drop on a video tape, followed by the digitisation of the recorded image at given times, as measured with a stop watch. We studied, by this rather cumbersome method, the adsorption of lecithin and cholesterol at the water — 1,2-dichlorethane interface. Since at that time we were also developing the line by line digitiser, we did not continue these experiments but the preliminary results obtained were in agreement with the literature[54] . That

It was only with the use of the line by line digitiser that we were able to acquire a sequence of frames, as described in paragraph § 3.3.5.2. To test the system, we measured the variation of the interfacial tension with time at the interface between an aqueous solution of cytochrome c and nitrobenzene.

This chapter only contains the results obtained for this interface. No theoretical treatment for the kinetics of adsorption and no discussion of the results are given here.

means that a sharp decrease of interfacial tension was observed for the lecithin solution, whereas no change in tension was observed for cholesterol.

5.2. Experimental

Horse heart cytochrome c (type VI) from Sigma was used without further purification. It was dissolved in a phosphate buffer solution (0.025 M KH_2PO_4, 0.025 M Na_2HPO_4, pH = 7.0) to a concentration of $2 \cdot 10^{-6}$ M. To verify that the cytochrome c did not react with nitrobenzene, several absorption spectra were run, first on a sample of a solution of cytochrome c and buffer in pure water and then on the same solution in water saturated with nitrobenzene. The spectra remained unchanged despite the presence of the nitrobenzene.

All the other chemicals were AnalaR grade reagents. All solutions were prepared with quadruply distilled water.

The data acquisition (cf. § 3.3.5.2.) was enabled as soon as a drop was formed. The time for the formation of a drop with the syringe was less than 3 seconds.

5.3. Results

Figure 5.1 shows the variation of the interfacial tension with time for the interface between an aqueous solution of cytochrome c at $2 \cdot 10^{-6}$ M in phosphate buffer and nitrobenzene. A measurement was performed every 5 seconds but only one point out of every 4 measured is shown in figure 5.1.

It appears that this curve is composed of two distinct parts, i.e. $0 < t < 4$ mins and $t > 4$ mins. In order to check whether the first part ($0 < t < 4$ mins) is representative of a diffusion controlled adsorption process, we plotted the variation of the interfacial tension against the square root of time, as shown in figure 5.2 .

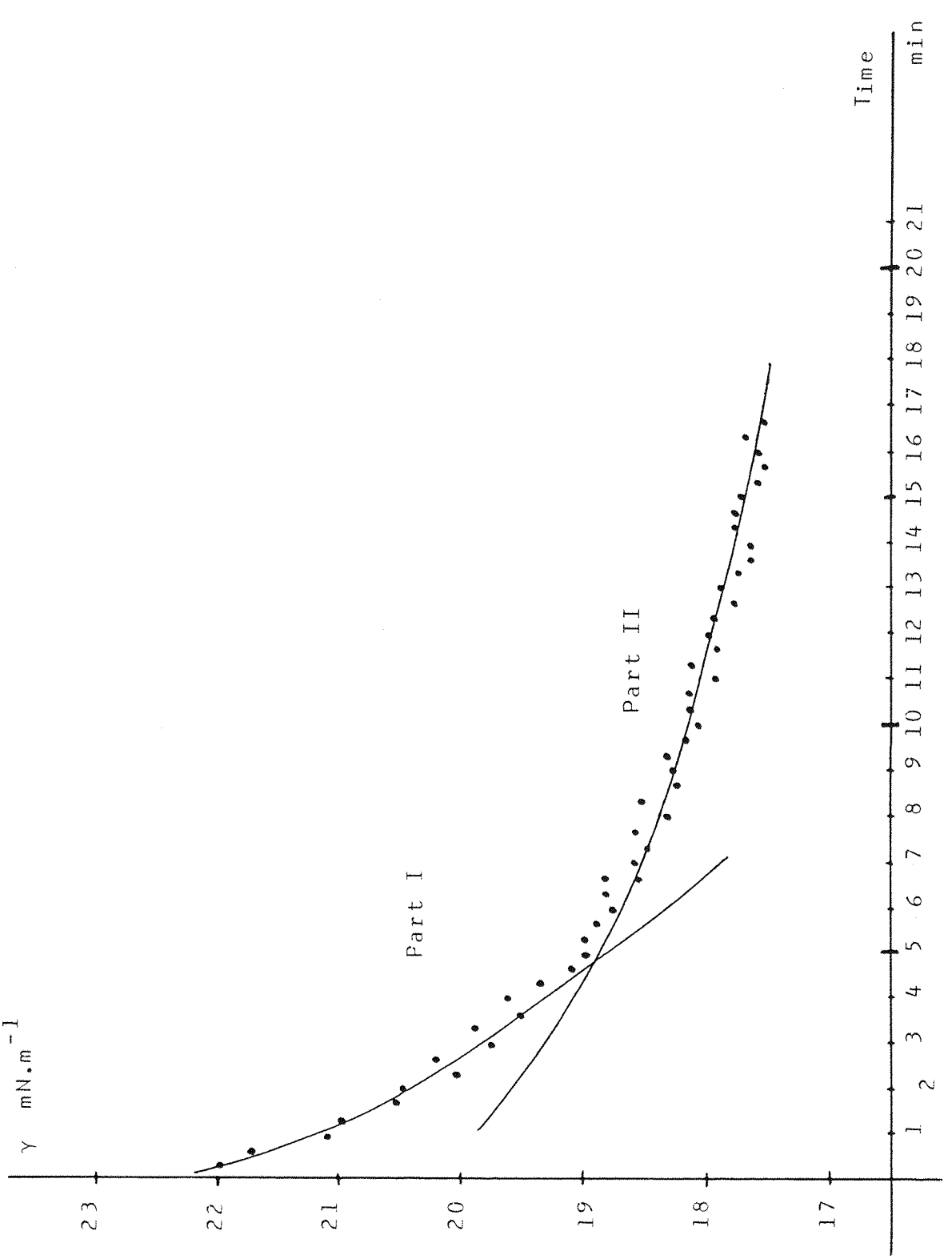
γ mN.m⁻¹
23
22
21
20
19
18
17
Part I
Part II
Time
min
1 2 3 4 5 6 7 8 9 10 11 12 13 14 15 16 17 18 19 20 21

Figure 5.1

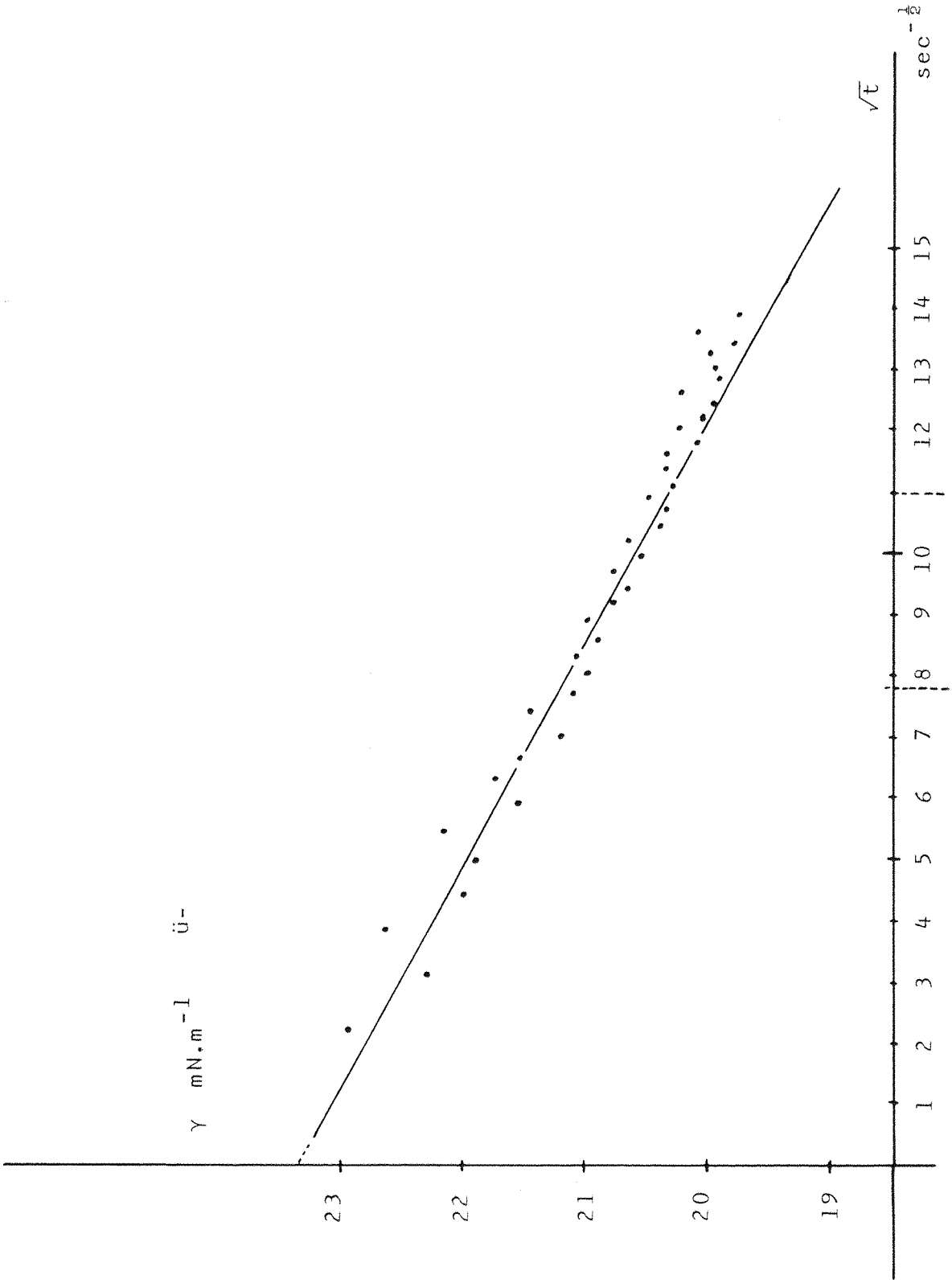

Figure 5.2

The linear behaviour indicates that the adsorbed cytochrom c forms an ideal non-localised monolayer. The equation of state for such a film is

$$\Pi\Omega = NRT \quad , \tag{5.1}$$

where $\Pi = \gamma - \gamma_0$ = surface pressure,
Ω = surface area,
N = number of molecules contained in the film.

The variation of N with time, in the absence of either an energy barrier or desorption was given by Ward and Tordai[68,69] as

$$\frac{N}{\Omega} = 2\, C_0 \sqrt{\frac{D\, t}{\pi}} \quad . \tag{5.2}$$

By substituting equation 5.2 into equation 5.1 , we have

$$\Pi = 2\, C_0\, RT \sqrt{\frac{D\, t}{\pi}} \quad . \tag{5.3}$$

The experimental results give, by linear regression, a slope of

$$\Pi = \gamma - \gamma_0 = 0.2804 \sqrt{t} \quad ,$$

which allows the estimation of the diffusion coefficient,

$$D = 2.5\ 10^{-5}\ cm^2\ sec^{-1} \quad .$$

This value is quite high compared with the value found in the literature ($10^{-6}\ cm^2\ sec^{-1}$)[52] . This decrepancy is most probably due to the simple model used here which completely ignores any desorption phenomenon and assumes an ideal two dimensional gas for the adsorbed phase. It is obvious that any further study should be assessed using a more complex model of adsorption.

5.4. Discussion

From the results shown, it appears that the data acquisition system of the digitised pendant drop video image is a very adequate static method of measurement of the boundary tension as a function of time. Measurements of adsorption at times greater than a few seconds may be undertaken with accuracy providing that the lowering of interfacial tension is not large enough to break the drop. According to paragraph § 2.3.5. the system of measurement is twice as accurate in measuring variations in the boundary tension than the absolute values and is therefore very appropriate to the measurements of kinetics phenomena. Furthermore, the line by line data acquisition system allows a continuous measurement of the area of the interface, monitoring thus, in this way, the enlargement of the surface due to the adsorption[66] . For times of adsorption less than a few seconds duration, we have to take into account the phenomena which occur during the formation of the drop (i.e. convection, adsorption, surface enlargement, etc.). Some attempts[42] have been made to evaluate these factors in the determination of the dynamic surface tension using the drop volume and maximum bubble pressure methods. Thus, it might be possible to develop a computational method capable of estimating fast adsorption processes during the drop formation.

PART IV

CHAPTER 6

CONCLUSION

6.1. Conclusions

The development of a digital technique for measuring boundary tension has opened wide the doors to the study of surface chemistry. The use we made of this system during this work can only be considered as a " running in " period. The technique combines the advantages of being computerised (too well known and too numerous to be listed here) and of the pendant drop methods which are the following.

a) It is an absolute method of measurement based on an exact mathematical treatment which does not introduce the use of tables or of correcting factors.

b) The locus of measurement is removed from any point of contact with materials other than the fluid.

c) Successive measurements of a given boundary may be made without disturbing that surface.

d) The boundary tensions of almost any magnitude may be measured.

These outstanding advantages, some of which are unique, may allow the investigation of many interfacial phenomena. The accuracy achieved has enabled us to measure water surface excess concentrations and an important consequence of this work is the observation that the ITIES does not contain two separate inner layers of solvent. Also, the data acquisition system has allowed us to measure the kinetics of adsorption of a protein at a liquid-liquid interface.

Furthermore, the automatic aspect of this technique makes it very well adapted to industrial applications such as quality control of wasted water, production optimisation, ...

6.2. Future work

The main objective in developing a novel technique for measuring interfacial tension was the study of the kinetics of charge transfer across membrane-like interfaces, formed by the adsorption of phospholipids and proteins at the interface of immiscible liquids. Indeed, Ohki[55] showed that a monolayer of phospholipid formed at the oil-water interface was a proper model system to represent the physical state of half a bilayer in its liquid crystalline state.

But charge transfer at the ITIES can mean either ion transfer or electron transfer. In this context, we hope to be able to study ion transfer across a monolayer in the same way as we did at the ITIES[25]. On the other hand, we will try to fix proteins such as cytochrom c on a phospholipid monolayer and observe whether electron transfer is feasible between the adsorbed cytochrome c and porphorin present in the non aqueous phase.

6.3. Postface or " Wink at Pr. Graham Hills "

In 1922, Heyrovsky wanted to measure the interfacial tension at the mercury-solution interface. He tried to adapt the drop weight method to this system and by this way he developed the dropping mercury electrode. Of course its utility far surpasses its original purpose and Heyrovsky won the Nobel Price.

Will the adaption of the pendant drop method to drop image processing techniques also surpass its original purpose ... ?

ANNEXE I

DROP IMAGE PROCESSING FOR SURFACE AND INTERFACIAL TENSION MEASUREMENTS

The following published papers were included in the bound thesis. These have not been digitised due to copyright restrictions, but the links are provided.

https://doi.org/10.1016/0022-0728(82)80036-3

ANNEXE II

PHYSICAL DATA

Specific Densities (10^3 kg • m^3)[38]

%	LiCl		NaCl		KCl	
	20° C	25° C	20° C	25° C	20° C	25° C
1	1.00411	1.00292	1.00534	1.00409	1.00463	1.00342
2	1.00993	1.00870	1.01246	1.01112	1.01103	1.00977
4	1.02148	1.02019	1.02680	1.02530	1.02391	1.02255
6	1.03296	1.03161	1.04127	1.03963	1.03690	1.03544
8	1.04443	1.04303	1.05589	1.05412	1.05003	1.04847
10	1.05594	1.05449	1.07068	1.06879	1.06332	1.06167
12	1.06752	1.06602	1.08566	1.08365	1.07679	1.07506
14	1.07919	1.07765	1.10085	1.09872	1.09046	1.08865
16	1.09098	1.08941	1.11621	1.11401	1.10434	1.10245
18	1.10292	1.10132	1.13190	1.12954	1.11845	1.11647
20	1.11504	1.11342	1.14779	1.14533	1.13280	1.13072
22	1.12736	1.12574	1.16395	1.16140	1.14740	1.14521
24	1.13991	1.13831	1.18040	1.17776	1.16226	1.15995
26	1.15271	1.15115	1.19717	1.19443	---	---
28	1.16578	1.16428	---	---	---	---
30	1.17914	1.17771	---	---	---	---

Molal Osmotic Coefficients ϕ and $\ell n\ a_{H_2O}$ at 25° C [57]

m	LiCl		NaCl		KCl		RbCl		CsCl	
	ϕ	$\ell n\ a$	ϕ	$\ell n\ a$	ϕ	$\ell n\ a$	ϕ	$\ell n\ a$	ϕ	$\ell n\ a$
0.1	0.939	0.00338	0.9324	0.00336	0.9266	0.00334	0.923	0.00332	0.917	0.00330
0.2	0.939	0.00676	0.9245	0.00666	0.9130	0.00657	0.907	0.00653	0.897	0.00646
0.3	0.945	0.01021	0.9215	0.00996	0.9063	0.00979	0.898	0.00970	0.885	0.00956
0.4	0.954	0.01374	0.9203	0.01327	0.9017	0.01298	0.893	0.01286	0.875	0.01260
0.5	0.963	0.01733	0.9209	0.01659	0.8989	0.01618	0.889	0.01600	0.869	0.01564
0.6	0.973	0.02102	0.9230	0.01995	0.8976	0.01939	0.887	0.01916	0.864	0.01866
0.7	0.984	0.02480	0.9257	0.02335	0.8970	0.02260	0.886	0.02233	0.861	0.02170
0.8	0.995	0.02750	0.9288	0.02677	0.8970	0.02583	0.886	0.02552	0.859	0.02474
0.9	1.006	0.03259	0.9320	0.03022	0.8971	0.02907	0.885	0.02867	0.858	0.02780
1.0	1.018	0.03665	0.9355	0.03370	0.8974	0.03231	0.885	0.03186	0.857	0.03058
1.2	1.041	0.04497	0.9428	0.04072	0.8986	0.03882	0.886	0.03828	0.856	0.03698
1.4	1.066	0.05373	0.9513	0.04793	0.9010	0.04541	0.888	0.04476	0.856	0.04314
1.6	1.091	0.06284	0.9616	0.05541	0.9042	0.05208	0.890	0.05126	0.857	0.04963
1.8	1.116	0.07232	0.9723	0.06305	0.9081	0.05884	0.893	0.05787	0.859	0.05566
2.0	1.142	0.08222	0.9833	0.07085	0.9124	0.06569	0.896	0.06451	0.864	0.06221
2.5	1.212	0.10908	1.0130	0.09117	0.9240	0.08316	0.905	0.08145	0.871	0.07839
3.0	1.286	0.13889	1.0453	0.11294	0.9367	0.10116	0.916	0.09893	0.880	0.09504
3.5	1.366	0.17212	1.0800	0.13608	0.9500	0.11970	0.928	0.11693	0.891	0.11227
4.0	1.449	0.20866	1.1158	0.16076	0.9647	0.13892	0.941	0.13550	0.901	0.12974
4.5	1.533	0.24835	1.1530	0.18679	0.9800	0.15876	0.952	0.15422	0.913	0.14791
5.0	1.619	0.29142	1.1916	0.21468	---	---	0.966	0.17388	0.923	0.16614
5.5	1.705	0.33759	1.2310	0.24374	---	---	---	---	0.934	0.18493
6.0	1.791	0.38686	1.2710	0.27454	---	---	---	---	0.945	0.20412

References:

1. M.H. Abraham and J. Liszi,
J. inorg. nucl. Chem., 43 (1981) 143.

2. M.H. Abraham, J. Liszi and E. Papp,
J. Chem. Soc.,Faraday Trans. I, 78 (1982) 197.

3. D.S. Abwani and T.J. Fort,
Surf. and Colloid Sci., 11 (1979) 93.

4. S.W. Amos and D.C. Birkinshaw,
Television Engineering, Vol. I, p. 252,
Iliffe & Sons, London, 1956.

5. J.D. Andreas, E.A. Hauser and W.B. Tucker,
J. Phys. Chem., 42 (1938) 1001.

6. F. Bashfort and J.C. Adams,
" An attempt to test the theories of Capillary action", University Press, Cambridge, 1883.

7. B.G. Batchelor, P.J. Brumfitt and B.D.V Smith,
" Command language for interactive image analysis",
IEEE Proc., 127 (1980) 203.

8. M. Blank,
J. Colloid Interface Sci., 22 (1966) 51.

9. D.J. Donahue and F.E. Bartell,
J. Phys. Chem., 56 (1952) 480.

10. M. Dupeyrat and J. Michel,
C. R. Acad. Sci. Ser. C, 264 (1967) 1240.

11. M. Dupeyrat and J. Michel,
J. Colloid Interface Sci., 29 (1969) 605.

12. M. Dupeyrat and E. Nakache,
J. Colloid Interface Sci., 73 (1979) 332.

13. F.M. Fowkes,
J. Phys. Chem., 67 (1963) 2538.

14. S. Fordham,
Proc. Roy. Soc., A194 (1948) 1.

15. H.S. Frank and M.W. Evans,
J. Chem. Phys., 13 (1945) 507.

16. C. Gavach, T. Mlodnicka and J. Guastalla,
C. R. Acad. Sci. Ser. C, 266 (1968) 1196.

17. C. Gavach and F. Henry,
C. R. Acad. Sci. Ser. C, 274 (1972) 1545.

18. C. Gavach and B. d'Epenoux,
J. Electroanal. Chem., 54 (1974) 361.

19. C. Gavach, F. Henry and R. Sandreaux,
C. R. Acad. Sci. Ser. C, 278 (1974) 491.

20. C. Gavach, P. Seta and F. Henry,
Bioelctrochem. and Bioenerg., 1 (1974) 329.

21. C. Gavach and B. d'Epenoux,
J. Electroanal. Chem., 55 (1974) 59.

22. C. Gavach, B. d'Epenoux and F. Henry,
J. Electroanal. Chem., 64 (1975) 107.

23. C. Gavach, P. Seta and B. d'Epenoux,
J. Electroanal. Chem., 83 (1977) 225.

24. W. Gibbs,
Scientific Papers, 1 (1878) 219.

25. H.H. Girault,
Diplôme d'Etudes Appprofondies, Institut National Polytechnique de Grenoble, 1980.

26. H.H. Girault, D.J. Schiffrin and B.D.V. Smith,
J. Electroanal. Chem., 137 (1982) 207.

27. M. Gros, S. Gromb and C. Gavach,
J. Electroanal. Chem., 89 (1978) 29.

28. J. Guastalla,
J. Chim. Phys., 53 (1956) 470.

29. J. Guastalla, A. Lize and N. Davion,
J. Chim. Phys., 68 (1971) 822.

30. J. Guastalla and C. Bertrand,
C. R. Acad. Sci. Ser. C, 274 (1972) 1884.

31. J. Guastalla and C. Bertrand,
C. R. Acad. Sci. Ser. C, 277 (1973) 279.

32. CRC. Handbook of Chemistry and Physics,
61st Edition, CRC Press Inc., Florida, 1980.

33. W.D. Harkins and F.E. Brown,
J. Am. Chem. Soc., 41 (1919) 499.

34. W.D. Harkins and H.M. Mc Laughlin,
J. Am. Chem. Soc., 47 (1925) 2083.

35. W.D. Harkins and E.C. Gilbert,
J. Am. Chem. Soc., 48 (1926) 604.

36. D. Homolka and V. Marecek,
J. Electroanal. Chem., 112 (1980) 91.

37. B. Hundhammer, T. Solomon and B. Alemayehu,
J. Electroanal. Chem., 135 (1982) 301.

38. International Critical Tables,
Mc Graw-Hill, New-York, 1933.

39. G. Jones and W.A. Ray,
J. Am. Chem. Soc., 59 (1937) 187.

40. G. Jones and W.A. Ray,
J. Am. Chem. Soc., 63 (1941) 288 & 3262.

41. G. Jones and W.A. Ray,
J. Am. Chem. Soc., 64 (1942) 2744.

42. P. Joos and E. Rillaerts,
J. Colloid Interface Sci., 79 (1981) 96.

43. Z. Koczorowski and G. Geblewicz,
J. Electroanal. Chem., 108 (1980) 117.

44. J. Koryta, P. Vanysek and M. Brezina,
J. Electroanal. Chem., 67 (1976) 263.

45. J. Koryta, P. Vanysek and M. Brezina,
J. Electroanal. Chem., 75 (1977) 211.

46. J. Koryta,
Electrochimica Acta, 24 (1979) 293.

47. J. Koryta and P. Vanysek,
in H. Gerischer and C.W. Tobias (Eds),
Advances in Electrochemistry and Electrochemical Engineering, Vol. 12, Wiley-Interscience, New York, 1982.

48. I. Langmuir,
J. Am. Chem. Soc., 39 (1917) 1883.

49. O.R. Melroy, R.P. Buck, F.S. Stover and H.C. Hughes,
J. Electroanal. Chem., 121 (1981) 93.

50. D.M. Mohilner and T. Kakiuchi,
J. Electrochem. Soc., 128 (1981) 350.

51. W. Nernst and E.H. Riesenfeld,
Ann. Phys., 8 (1902) 600.

52. K. Niki, T. Yagi, H. Inokuchi and K. Kimura,
J. Am. Chem. Soc., 101 (1979) 3335.

53. P.L. du Noüy,
J. Gen. Physiol., 1 (1919) 521.

54. K. Ogino and M. Onishi,
J. Colloid Interface Sci., 74 (1981) 18.

55. S. Ohki, C.B. Ohki and N. Duzgunes,
Colloid Interface Sci. (Proc. Int. Conf. 50th),
5 (1976) 271.

56. J.E.B. Randles,
in P. Delahay and C.W. Tobias (Eds),
Advances in Electrochemistry and Electrochemical Engineering, Vol. 3, Wiley-interscience,New York, 1963.

57. D.A. Robinson and R.H. Stokes,
Electrolyte Solutions, 2nd Edition, Butterworths Scientific Publications, London, 1959.

58. R.J. Roe,
J. Colloid Interface Sci., 31 (1969) 228.

59. Z. Samec, V. Marecek, J. Koryta and M.W. Khalil,
J. Electroanal. Chem., 83 (1977) 393.

60. Z. Samec, V. Marecek, J. Weber and D. Homolka,
J. Electroanal. Chem., 99 (1979) 385.

61. Z. Samec, V. Marecek and J. Weber,
J. Electroanal. Chem., 100 (1979) 841.

62. Z. Samec, V. Marecek and D. Homolka,
J. Electroanal. Chem., 126 (1981) 121.

63. D.J. Schiffrin,
J. Electroanal. Chem., 23 (1969) 168.

64. C.E. Stauffer,
J. Phys. Chem., 69 (1965) 1933.

65. T. Tate,
Phil. Mag., 27 (1864) 176.

66. E. Tornberg and G. Lundh,
J. Colloid Interface Sci., 79 (1981) 76.

67. H. Vos and J.M. Los,
J. Colloid Interf. Sci., 74 (1980) 360.

68. A.F.H. Ward and L. Tordai,
Rec. Tra. Chim., 71 (1952) 396.

69. A.F.H. Ward and L. Tordai,
J. Chem. Phys., 14 (1946) 453.

70. A. Watanabe, M. Matsumoto, H. Tamai and R. Gotah,
Kolloid-Z. & Z. Polym., 220 (19

71. Wilhelmy,
Ann. Phys., 119 (1863) 177.

72. A.M. Worthington,
Proc. Roy. Soc. London, 32 (1881) 362.

73. W.M. Gentleman,
Computer J., 12 (1969) 160.

74. C.W. Clenshaw,
Computer J., 2 (1960) 170.